

HOLISMOKEs. VIII. High-redshift Strong Lens Candidates from the Hyper Suprime-Cam Subaru Strategic Program

Yiping Shu^{1,2}, Raoul Cañameras¹, Stefan Schuldt^{1,3}, Sherry H. Suyu^{1,3,4}, Stefan Taubenberger¹, Kaiki Taro Inoue⁵, and Anton T. Jaelani⁶

¹ Max-Planck-Institut für Astrophysik, Karl-Schwarzschild-Str. 1, 85748 Garching, Germany
e-mail: ypshu@mpa-garching.mpg.de

² Ruhr University Bochum, Faculty of Physics and Astronomy, Astronomical Institute (AIRUB), German Centre for Cosmological Lensing, 44780 Bochum, Germany

³ Technische Universität München, Physik Department, James-Franck Str. 1, 85748 Garching, Germany

⁴ Institute of Astronomy and Astrophysics, Academia Sinica, 11F of ASMAB, No.1, Section 4, Roosevelt Road, Taipei 10617, Taiwan

⁵ Faculty of Science and Engineering, Kindai University, Higashi-Osaka, 577-8502, Japan

⁶ Astronomy Research Group and Bosscha Observatory, FMIPA, Institut Teknologi Bandung, Jl. Ganeshha 10, Bandung 40132, Indonesia

Received xxx; accepted xxx

ABSTRACT

We carry out a dedicated search for strong-lens systems with high-redshift lens galaxies with the goal of extending strong lensing-assisted galaxy evolutionary studies to earlier cosmic time. Two strong-lens classifiers are constructed from a deep residual network and trained with datasets of different lens redshift and brightness distributions. We classify a sample of 5,356,628 pre-selected objects from the Wide layer fields in the second public data release of the Hyper Suprime-Cam Subaru Strategic Program (HSC-SSP) by applying the two classifiers to their HSC *gri*-filter cutouts. Cutting off at thresholds that correspond to a false-positive rate of 10^{-3} on our test set, the two classifiers identify 5,468 and 6,119 strong-lens candidates. Visually inspecting the cutouts of those candidates results in 735 grade-A/B strong-lens candidates in total, of which 277 candidates are discovered for the first time. This is the single largest set of galaxy-scale strong-lens candidates discovered with HSC data to date, and nearly half of it (331/735) contains lens galaxies with photometric redshifts above 0.6. Our discoveries will serve as a valuable target list for ongoing and scheduled spectroscopic surveys such as the Dark Energy Spectroscopic Instrument, the Subaru Prime Focus Spectrograph project, and the Maunakea Spectroscopic Explorer.

Key words. Galaxies: evolution – Gravitational lensing: strong – Methods: data analysis

1. Introduction

The strong gravitational lensing effect is a powerful and robust mass probe that can deliver few-percent level measurements of the total mass (including dark matter) in the central regions of galaxies at extragalactic distances. Studies using strong lensing alone or in combination with other constraints have successfully measured dark matter and stellar mass distributions and their evolution in distant galaxies, which have deepened our understanding on galaxy formation and evolution (e.g., Treu et al. 2006; Koopmans et al. 2006; Auger et al. 2010; Bolton et al. 2012a; Brewer et al. 2014; Shu et al. 2015, 2016c). Detections of dark-matter substructures beyond the local Universe have accumulated and measurements of the substructure mass from strong-lensing observables have placed constraints on the subhalo mass function and the nature of dark matter (e.g., Vettetti et al. 2010, 2012; Fadely & Keeton 2012; Nierenberg et al. 2014; Hezaveh et al. 2016; Inoue et al. 2016). In addition, the lensing magnification effect has been exploited to overcome the sensitivity and/or resolution limitations of current facilities and provide detailed dissections of high-redshift objects (e.g., Christensen et al. 2012; Bussmann et al. 2013; Stark et al. 2015; Shu et al. 2016b; Marques-Chaves et al. 2017, 2018, 2020; Shu

et al. 2021a). Moreover, strongly-lensed variable sources, such as quasars and supernovae (SNe), have evolved into an independent and compelling cosmological probe (e.g., Suyu et al. 2010, 2013, 2017; Grillo et al. 2018; Wong et al. 2020; Millon et al. 2020), which is one of the main motivations for our Highly Optimised Lensing Investigations of Supernovae, Microlensing Objects, and Kinematics of Ellipticals and Spirals (HOLISMOKEs) programme (Suyu et al. 2020).

Various techniques have been developed to identify the intrinsically rare strong-lens systems. The most productive to date are imaging-based methods, which have discovered ≈ 400 strong-lens systems¹ (e.g., Browne et al. 2003; More et al. 2012; Stark et al. 2013; Pawase et al. 2014; Sonnenfeld et al. 2018; Lemon et al. 2018; Shu et al. 2018b, 2019; Chan et al. 2020; Desira et al. 2022). Over the past two decades, spectroscopy-based methods have heavily exploited large-scale spectroscopic surveys and discovered more than 200 strong-lens systems (e.g., Bolton et al. 2004, 2008; Treu et al. 2011; Brownstein et al. 2012; Courbin et al. 2012; Shu et al. 2016b,c; Oldham et al. 2017; Shu et al. 2017). Very recently, variability-based methods, which are particularly useful for discovering strongly-lensed

¹ According to <http://admin.masterlens.org/index.php>

variable sources such as quasars, have gained momentum and will undoubtedly play a crucial role in the ongoing and upcoming time-domain surveys (e.g., Kostrzewska-Rutkowska et al. 2018; Chao et al. 2020, 2021; Shu et al. 2021b; Bag et al. 2021).

Although the total number of confirmed strong-lens systems have reached $\approx 600^1$, many scientific applications call for more systems and a more thorough coverage of the phase space. For example, a lot of efforts have been made to search for strongly-lensed SNe, which are expected to provide tighter constraints on the Hubble constant compared with strongly-lensed quasars (e.g., Oguri & Kawano 2003; Goldstein & Nugent 2017; Wojtak et al. 2019; Huber et al. 2021a,b; Bayer et al. 2021; Ding et al. 2021). Two efficient approaches of catching such rare and short-lived lensing events are crossmatching transient alerts from time-domain surveys with known strong-lens systems and carrying out dedicated monitorings of known strong-lens systems with high expected lensed SN rates (e.g., Shu et al. 2018a; Ryczkowski et al. 2020; Craig et al. 2021), both of which benefit greatly from discovering more strong-lens systems. Additionally, strong lensing-assisted evolutionary analyses have so far been limited to low- and intermediate-redshift galaxies due to the lack of galaxy-galaxy strong-lens systems with high-redshift lens galaxies. Among all confirmed galaxy-galaxy strong-lens systems, only a handful contain lens galaxies at redshifts beyond 0.8 (e.g., Wong et al. 2014; Cañameras et al. 2017). On the other hand, high-redshift galaxies are crucial in understanding galaxy evolution as they are expected to undergo more frequent and vigorous transitions. Recently, the combination of wide-field imaging surveys and machine learning algorithms has led to a big leap in strong lens discoveries. A few thousand new strong-lens candidates have been uncovered by classifiers built upon supervised or unsupervised algorithms (e.g., Jacobs et al. 2019a; Petrucci et al. 2019; Cañameras et al. 2020, 2021; Huang et al. 2020; Li et al. 2020; Huang et al. 2021; Li et al. 2021; Stein et al. 2021; Rojas et al. 2021; Savary et al. 2021). Future surveys, such as the Rubin Observatory Legacy Survey of Space and Time (LSST, Ivezić et al. 2019), Euclid (Laureijs et al. 2011), and the Chinese Space Station Optical Survey (CSS-OS, Zhan 2018), expect to deliver $\sim 10^5$ strong-lens systems (e.g., Collett 2015).

In this work, we focus on extending strong lensing-assisted evolutionary analyses to earlier cosmic time by searching for high-redshift strong lenses in the Wide layer data from the second public data release (PDR2) of the Hyper Suprime-Cam Subaru Strategic Program (HSC-SSP, Aihara et al. 2019). In Section 2, we describe the HSC-SSP PDR2 data and define our parent sample. Section 3 explains the construction and training of our two strong-lens classifiers based on a deep residual network, and the performance of the two classifiers is shown in Section 4. Discovered strong-lens candidates are presented in Section 5. Six candidates that show two sets of spectral features at different redshifts in auxiliary spectroscopic data are reported in Section 6. Discussions and conclusions are provided in Section 7 and 8. To compute the Einstein radii, we adopt a flat Λ CDM cosmology with $\Omega_m = 1 - \Omega_\Lambda = 0.32$ (Planck Collaboration et al. 2020) and $H_0 = 72 \text{ km s}^{-1} \text{ Mpc}^{-1}$ (Bonvin et al. 2017).

2. Data

In HSC-SSP PDR2, the Wide layer data cover $\approx 300 \text{ deg}^2$ in all five filters (i.e. *grizy*) to the nominal depths and additional $\approx 1,100 \text{ deg}^2$ in at least one filter and one exposure. The median 5σ depths (for point sources) in *grizy* filters for the PDR2 Wide layer are 26.6, 26.2, 26.2, 25.3, and 24.5 mag and the median seeings are 0''.77, 0''.76, 0''.58, 0''.68, 0''.68 respectively. A

full overview of HSC-SSP PDR2 can be found in Aihara et al. (2019). For our high-redshift strong-lens search, we select objects that are extended and likely located at high redshifts based on their $g-r$ and $g-i$ colours. To be more specific, we select objects in the `pdr2_wide.forced` table that satisfy the following criteria:

1. `isprimary` is True
2. `i_extendedness_value=1`
3. `[grizy]_sdsscentroid_flag` is False
4. `[grizy]_pixelflags_edge` is False
5. `[grizy]_pixelflags_interpolatedcenter` is False
6. `[grizy]_pixelflags_saturatedcenter` is False
7. `[grizy]_pixelflags_crcenter` is False
8. `[grizy]_pixelflags_bad` is False
9. `[grizy]_cmodel_flag` is False
10. `g_cmodel_mag < 26.0`
11. `r_cmodel_mag < 26.0`
12. `i_cmodel_mag < 26.0`
13. $0.6 < g_cmodel_mag - r_cmodel_mag < 3.0$
14. $2.0 < g_cmodel_mag - i_cmodel_mag < 5.0$

This query returns 5,356,628 unique HSC objects in total, which form the parent sample of this lens search project. Here criteria 3–12 are used to remove objects with unreliable photometry (e.g., Tanaka et al. 2018; Schuldt et al. 2021a), and the colour-colour cuts in criteria 13–14 are directly taken from Jacobs et al. (2019b) to select red and potentially high-redshift galaxies. We find that criteria 13–14 manage to substantially reduce the sample size and at the same time maintain a high completeness rate for high-redshift lens galaxies. Removing criteria 13–14 in the above query will result in a sample of 79,577,619 unique extended objects, which would have posed challenges to not only the final lens search but also the initial imaging data retrieval. On the other hand, Jacobs et al. (2019b) simulated 10,000 $z > 0.8$ elliptical galaxies with lensed features superimposed, and found that $\gtrsim 90\%$ of the simulated lenses can be recovered with these two colour-colour cuts. In addition, we examine the colour distributions of strong-lens candidates discovered in the HSC footprint by the Survey of Gravitationally-lensed Objects in HSC Imaging (SuGOHI) project (Sonnenfeld et al. 2018; Wong et al. 2018; Chan et al. 2020; Jaelani et al. 2020; Sonnenfeld et al. 2020). Every SuGOHI strong-lens candidate is assigned a grade from A (definite), B (probable), or C (possible) and a lens type from GG (galaxy-galaxy), GQ (galaxy-quasar), CG (cluster/group-galaxy), or CQ (cluster/group-quasar). As we are particularly interested in galaxy-galaxy strong lenses, we focus on the 99 SuGOHI grade-A/B GG strong-lens candidates that have lens galaxies fulfilling criteria 1–12. The lens galaxies in those strong-lens candidates are primarily luminous red galaxies selected according to the criteria defined in Dawson et al. (2013). They span a wide redshift range from 0.2 to 1.0². We note that candidates from Sonnenfeld et al. (2020) are not considered here because some GG strong-lens candidates therein are actually cluster- or group-scale lenses. Among the selected 99 SuGOHI strong-lens candidates, 92 (or $\approx 93\%$) further pass the colour-colour cuts in criteria 13–14. Limiting to the selected SuGOHI candidates with lens galaxy (spectroscopic/photometric) redshifts above 0.8, 4/5 (or 80%) pass the colour-colour cuts. Although the colour-colour cuts were originally defined in the photometric system of the Dark Energy Survey, we expect them to be similarly effective in the HSC photometric system given

² According to the spectroscopic or photometric redshifts available on <http://www-utap.phys.s.u-tokyo.ac.jp/~oguri/sugohi/>

the minor difference between them (Abbott et al. 2021) and the encouraging results from the SuGOHI sample.

HSC *gri*-filter cutouts ($72 \text{ pixels} \times 72 \text{ pixels}$, 1 pixel = $0''.17$) centred on those 5,356,628 objects are retrieved from the PDR2 Image Cutout service. Photometry (CModel magnitudes from the `pdr2_wide.forced` table, Aihara et al. 2019) and photometric redshift (`photoz_best` from the `pdr2_wide.photoz_mizuki` table, Tanaka et al. 2018) for every object in the parent sample are also retrieved from the HSC CAS Search service. The parent sample covers roughly 960 deg^2 .

3. Strong-lens Classifier Construction

We construct two strong-lens classifiers based on the deep residual network, `deeplens_classifier`, pre-built in the CMU DeepLens package (Lanusse et al. 2018). Deep residual networks (resnets), a variation of convolutional neural networks, have become the current state-of-the-art imaging recognition algorithm, and CMU DeepLens adopts a specific resnet architecture proposed by He et al. (2016). Among the nine different lens-finding methods in the Strong Gravitational Lens Finding Challenge, CMU DeepLens delivered the highest area under the receiver operating characteristic curve (AUROC) value, which is the most commonly used evaluation metric for classification problems (Metcalf et al. 2019). It is also top-ranked on the other two metrics considered. We therefore choose `deeplens_classifier` from CMU DeepLens as our baseline model, and a full description of the network architecture can be found in Lanusse et al. (2018). The `deeplens_classifier` network is constructed such that it returns a number from 0 to 1 for every input system, which is referred to as the network score p_{resnet} .

The `deeplens_classifier` network takes several parameters that determine how the actual training is done. In particular, `learning_rate` sets the initial learning rate, `learning_rate_steps` sets the number of learning rate updates during training, `learning_rate_drop` sets the amount by which the learning rate is updated, and `n_epochs` sets the total number of training epochs. For example, the network that delivered the highest AUROC value in the Strong Gravitational Lens Finding Challenge had `learning_rate= 0.001`, `learning_rate_steps= 3`, `learning_rate_drop= 0.1`, and `n_epochs= 120`, which correspond to a starting learning rate of 0.001 that is multiplied by 0.1 every 40 epochs. In this work, we always use a `learning_rate_drop` of 0.1. The two strong-lens classifiers presented in this work mainly differ in the training set and the `learning_rate`, `learning_rate_steps`, and `n_epochs` parameters.

3.1. Classifier-1

3.1.1. Training/validation Dataset

As the total number of confirmed strong lenses is on the order of 10^3 , mock lens systems needs to be created for training and validation. We try to be as realistic as possible by using observed data of real galaxies to make the mock systems. Following Cañameras et al. (2021, C21 hereafter), we select $\approx 80,000$ galaxies in the Data Release 14 of the Sloan Digital Sky Survey (Abolfathi et al. 2018) that are also in the HSC footprint and have measured spectroscopic redshifts and velocity dispersions (Bolton et al. 2012b) as the lens sample. We directly take HSC *gri*-filter cutouts ($72 \text{ pixels} \times 72 \text{ pixels}$) centred on those lens

galaxies as the base layer. As a result, mock lens systems naturally include various observational effects, such as galaxy colour gradients, seeing variations, neighbouring and line-of-sight contaminants, and artefacts, that are also present in the parent sample. To further enlarge the lens sample, we rotate every galaxy in the lens sample by 90° , 180° , and 270° , and consider them as different lens galaxies. This implies that each galaxy in the lens sample is used at most four times. For the source sample, we use $\approx 1,300$ high signal-to-noise ratio (S/N) galaxies in the Hubble Ultra Deep Field with secure spectroscopic redshifts (Inami et al. 2017). We convert images of the selected source galaxies in HST bands (F435W, F606W, and F775W) to HSC *gri* filters using the method in Cañameras et al. (2021).

Similar to procedures used in Cañameras et al. (2020, 2021) and Schuldt et al. (2021b), we model the effective lensing potential as two components, a projected lens mass component characterised by a singular isothermal ellipsoid (SIE) profile and an external shear. The axis ratio and position angle of the SIE profiles are set to values inferred from the lens surface-brightness distribution in the HSC *i* band. The external shear strength is randomly drawn from a Gaussian distribution with mean 0 and standard deviation 0.058 (e.g., Wong et al. 2011; Faure et al. 2011) and the position angle is randomly chosen from 0° to 180° . For every lens galaxy, we randomly pair it with a galaxy from the source sample that is at a redshift higher than the lens galaxy. The Einstein radius of the SIE profile can now be computed from the lens and source redshifts and the lens velocity dispersion. The selected source galaxy is randomly placed with a requirement that its centroid needs to be at a location with a total magnification of 5 or greater. We use GLEE (e.g., Suyu & Halkola 2010; Suyu et al. 2012) to generate the lensed image of the source, which is further downsampled to the HSC pixel size and convolved with the point spread function (PSF) at the location of the lens provided by the HSC PSF picker. We require that the brightest pixel in the lensed image to be brighter than the corresponding pixel value in the base layer in either *g*- or *i*-band. Otherwise, we draw a new source position, generate the lensed image, and compare. This process can be iterated for at most 40 times, after which the brightness of the selected source galaxy is boosted by 0.5 mag in all three bands and the whole process is repeated. If the requirement is still not satisfied after boosting the selected source by 5 mag, a new source galaxy is selected. Once the requirement is satisfied, the lensed image is added to the base layer to produce the composite image of a mock lens system.

For this first classifier, we specifically select 43,500 mock lens systems that produce a close to uniform Einstein radius distribution between $0''.75$ and $2''.5$ as positive examples. The Einstein radius is the single most important quantity of a strong-lens system, and is determined primarily by the lens galaxy mass with an additional dependence on the lens and source redshifts. We choose a uniform Einstein radius distribution so that the classifier is equally sensitive to strong-lens systems with different lens galaxy mass and lens/source redshifts. To ensure the translation invariance of the classifier, we extract for each mock lens system a $60 \text{ pixels} \times 60 \text{ pixels}$ *gri* cutout randomly centred within ± 5 pixels in both R.A. and Decl. directions of the center of the original cutout ($72 \text{ pixels} \times 72 \text{ pixels}$), and refer to the 43,500 cutouts as the lens data set. As indicated by Figure 1, the redshift distribution of lens galaxies in this training set is peaked at ≈ 0.55 . The *i*-band magnitude distribution of lens galaxies is peaked at ≈ 19.5 mag and drops rapidly towards the faint side. In fact, the magnitude distribution of the lens galaxies, which are all spectroscopically-observed galaxies in the SDSS surveys,

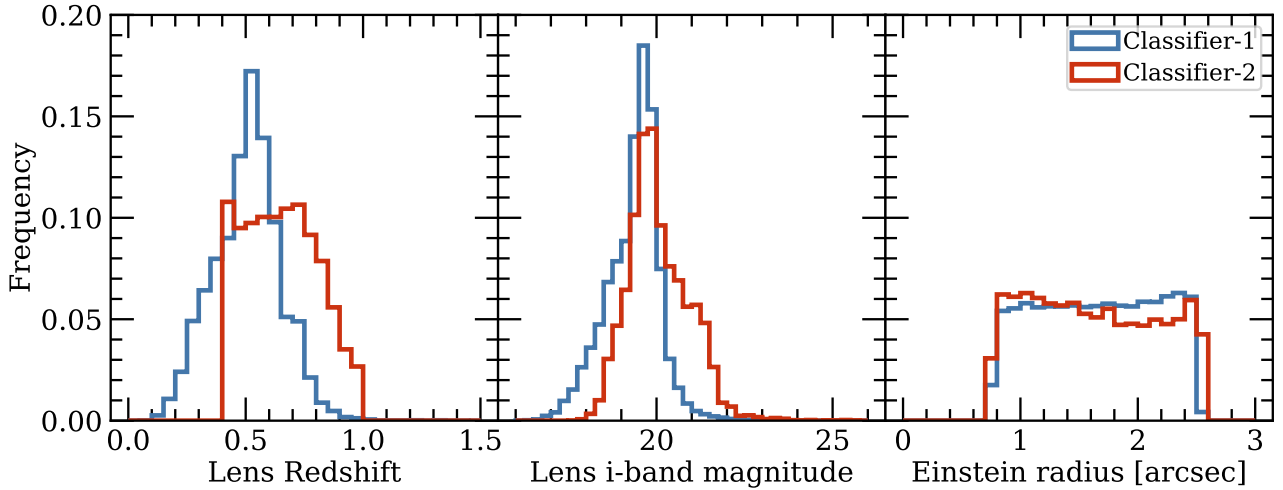


Fig. 1: Distributions of lens galaxy redshift, lens galaxy i -band magnitude, and Einstein radius for mock lenses in the training sets for Classifier-1 (blue) and Classifier-2 (red).

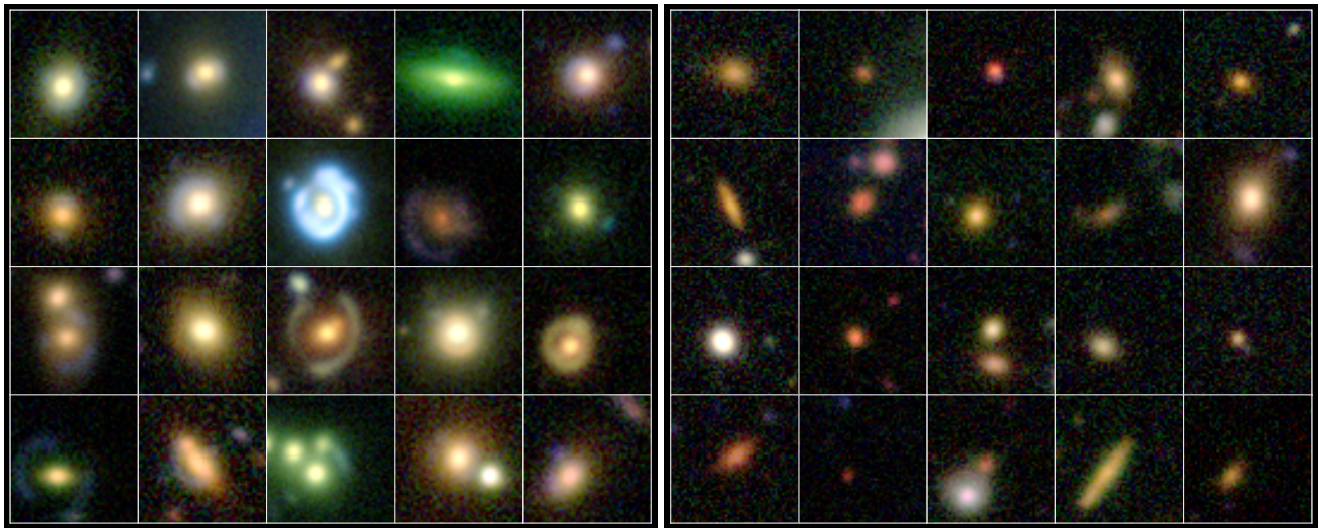


Fig. 2: Colour composite images of 20 mock lenses (left) and 20 non-lens examples (right) randomly selected from the training set for Classifier-1.

is primarily due to SDSS selection effects. In SDSS-III, galaxies selected for spectroscopic observations are all brighter than $i < 19.9$ (Dawson et al. 2013), and the faint limit for galaxy target selection extends to $i \leq 21.8$ in SDSS-IV (Prakash et al. 2016).

To construct the non-lens examples for training and validation, we first randomly select 48,213 objects from the parent sample. To further clean this subset, we crossmatch them with a sample of 10,241 known strong lenses and strong-lens candidates (referred to as the known strong lens compilation hereafter) compiled from the literature (e.g., Diehl et al. 2017; Sonnenfeld et al. 2018; Wong et al. 2018; Petrillo et al. 2019; Jacobs et al. 2019b,a; Chan et al. 2020; Jaelani et al. 2020; Sonnenfeld et al. 2020; Huang et al. 2020, 2021; Cañameras et al. 2020; Li et al. 2020; Cañameras et al. 2021; Li et al. 2021; Rojas et al. 2021; Savary et al. 2021) using a matching radius of 30 arcsecs and remove the 114 matches. Considering the typical lensing rate of 10^{-4} – 10^{-3} (e.g., Browne et al. 2003; Bolton et al. 2004; Oguri & Marshall 2010; Treu 2010), the remaining 48,099 objects are expected to be sufficiently pure. Among them, 43,500 objects are

randomly selected as the final non-lens examples (to match the size of the lens data set). Similarly, a random shift within ± 5 pixels in both directions is applied simultaneously to the gri -filter cutouts of each non-lens example. The shifted gri -filter cutouts of the 43,500 objects are trimmed to 60 pixels \times 60 pixels and form the non-lens data set.

The lens and non-lens data sets are merged into a single dataset, which is then randomly shuffled. 80% of the shuffled dataset is used for training and the remaining 20% is used for validation. Twenty mock lens systems and twenty non-lens systems randomly selected from the training set are shown in Figure 2 as an illustration.

3.1.2. Test Dataset

To construct the non-lens examples for the test set, we first randomly select 53,570 objects from the parent sample. To further clean this subset, we crossmatch it with the known strong lens compilation from the previous step and the 43,500 non-lens examples used for training and validation using a matching radius

of 30 arcsecs and remove the 152 and 1,649 matches. 50,000 objects are randomly selected from the remaining objects, and their *gri*-filter cutouts are trimmed to 60 pixels \times 60 pixels and form the non-lens examples of the test set.

To construct the lens examples for the test set, we use strong lenses and strong-lens candidates from the SuGOHI project. The SuGOHI project has discovered 2,002 strong lenses and strong-lens candidates based on HSC imaging data (Sonnenfeld et al. 2018; Wong et al. 2018; Chan et al. 2020; Jaelani et al. 2020; Sonnenfeld et al. 2020), of which 1,411 systems pass our selection criteria in Section 2 and are included in our parent sample. As we are particularly interested in our network's ability in discovering galaxy-galaxy strong lenses, we only include in the test set 23 grade-A and 69 grade-B galaxy-galaxy strong-lens candidates from the 1,411 SuGOHI systems. Again, their *gri*-filter cutouts are trimmed to 60 pixels \times 60 pixels and form the lens examples of the test set. For the sake of simplicity, candidates from Sonnenfeld et al. (2020) are also not included in this step because some classified GG strong-lens candidates therein are actually cluster- or group-scale systems.

3.1.3. Network Tuning

To quantify the network performance, we examine the true positive rate (TPR) and false positive rate (FPR). The TPR and FPR are defined as:

$$\text{TPR} = \frac{\text{Number of lenses that are correctly classified as lenses}}{\text{Number of lenses in a dataset}}, \quad (1)$$

$$\text{FPR} = \frac{\text{Number of non-lenses that are mis-classified as lenses}}{\text{Number of non-lenses in a dataset}}. \quad (2)$$

As mentioned previously, the network performance is usually measured by the AUROC metric for such a classification problem. The receiver operating characteristic (ROC) curve is the relation between TPR and FPR when the network score threshold varies from 0 to 1, and the AUROC is the integration of the ROC curve. For reference, a perfect classifier has an AUROC of 1.0, which is the best possible value, and a classifier that makes random predictions has an AUROC of 0.5.

For this classifier, we explore three different options for network parameters `learning_rate`, `learning_rate_steps`, and `n_epochs`. The first option corresponds to the default values that delivered the highest AUROC value in the Strong Gravitational Lens Finding Challenge, i.e. [0.001, 3, 120] (in the format of [`learning_rate`, `learning_rate_steps`, `n_epochs`]). The other two options are [0.01, 4, 160] and [0.1, 5, 200]. The network that is trained with [0.01, 4, 160] has the highest AUROC on the test dataset, and is therefore chosen to be the final network for Classifier-1.

3.2. Classifier-2

3.2.1. Training/validation Dataset

As the ultimate goal of this work is finding high-redshift strong lenses, we experiment with a different training set that contains a higher fraction of high-redshift ($z \gtrsim 0.6$) lenses compared to the training set used for Classifier-1. We use the same procedures outlined in Section 3.1.1 to create mock lenses. The only difference is, we now manually adjust the redshift distribution

of the lens galaxies to a relatively uniform distribution from 0.4 to 1.0 (Figure 1) when creating the mocks. Because the number of $z > 0.8$ galaxies in the lens sample is relatively small and each galaxy is only used at most four times, the total number of mock lens systems is now 28,500. We therefore augment the mock lens sample by vertically flipping the cutouts of the 28,500 mock lens systems and consider them as new mock lens systems. 56,960 mock systems are then randomly selected from those 57,000 systems, which are used as the final sample of mock lenses. This new set of mocks has a similar close to uniform Einstein radius distribution but clearly contains a higher fraction of fainter lens galaxies as indicated in Figure 1. For the non-lens examples, we randomly select another 56,960 objects from the parent sample that do not have counterparts in the known strong lens compilation and the test set for Classifier-1. The randomly shifted *gri*-filter cutouts (60 pixels \times 60 pixels) of the 113,920 mock lenses and non-lens examples are merged into a single dataset, which is again randomly shuffled.

In addition, two pre-processing steps are introduced. We first take the square root of the absolute value of the dataset. Considering that the lensed features are expected to be fainter than the lens galaxies in general, this square-root stretch step improves the contrast between the lens galaxy and lensed features, which has been found to improve the performance of the network (Cañameras et al., in prep.). Afterwards, we normalise the cutouts of every system in the dataset so that the brightest pixel in the individual filter is always 1.

Moreover, instead of one network, Classifier-2 is composed of ten networks that are trained with different training sets. This is achieved by implementing the k-fold cross validation process. More specifically, the single dataset mentioned above is divided into ten chunks of equal size. Each of the ten chunks is used consecutively as the validation set and the remaining nine chunks are used to train a network. In total, ten networks are obtained, and the average of their output p_{resnet} is used as the final p_{resnet} for every input system.

3.2.2. Test Dataset

The same 92 lens and 50,000 non-lens examples introduced in Section 3.1.2 are used to construct the test dataset for Classifier-2. The only difference is, their *gri*-filter cutouts also undergo the square-root stretch and normalisation steps.

3.2.3. Network Tuning

Similarly, we consider three different options of network parameters `learning_rate`, `learning_rate_steps`, and `n_epochs`, i.e. [0.001, 3, 120], [0.01, 4, 160], and [0.1, 5, 150]. The set of ten networks that are trained with [0.1, 5, 150] delivers the highest AUROC on the test dataset, and is chosen as the final network set for Classifier-2.

4. Classifier Performances

Figure 3 shows the ROC curves for Classifier-1 (blue) and Classifier-2 (red) based on the test dataset. Classifier-1 has an AUROC of 0.993 and Classifier-2 has an AUROC of 0.985. For reference, the highest AUROC reported in the Strong Gravitational Lens Finding Challenge was 0.98 (Metcalf et al. 2019). Cañameras et al. (2020) obtained an AUROC of 0.985 and Huang et al. (2021) obtained an AUROC of 0.992. Although the AUROC values from different work cannot be directly compared

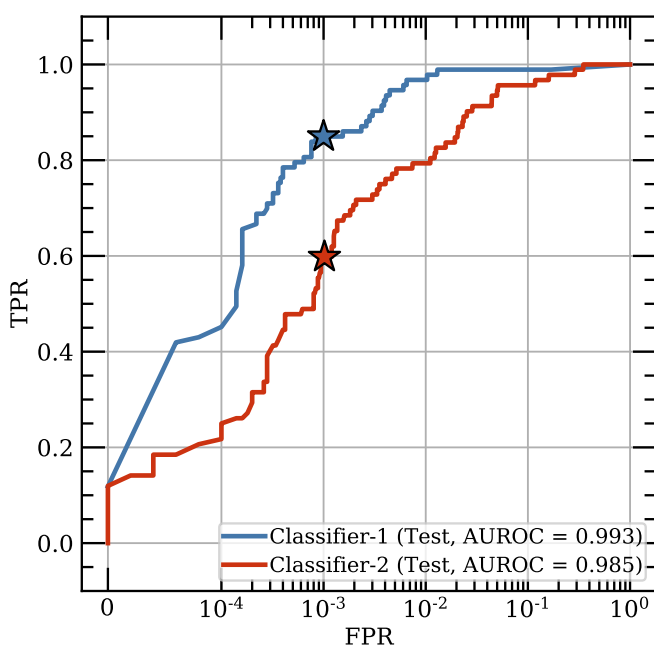


Fig. 3: ROC curves based on the test sets for Classifier-1 (blue) and Classifier-2 (red). The x-axis is scaled such that $0-10^{-4}$ is in a linear scale and $10^{-4}-1$ is in a logarithmic scale. The two star symbols correspond to $\text{FPR} = 10^{-3}$.

because they are evaluated on different test sets, our AUROC values being in the ballpark of the highest values achieved by recent strong lens classifiers based on neural networks suggests that our two classifiers have been well trained.

For each classifier, we select a p_{resnet} threshold that delivers an FPR of 10^{-3} as the fiducial threshold. Considering the typical strong-lensing rate of $10^{-4}-10^{-3}$ (e.g., Browne et al. 2003; Bolton et al. 2004; Oguri & Marshall 2010; Treu 2010), an FPR of 10^{-3} can ensure a reasonable balance between true positives and false positives. In addition, ≈ 6000 objects in our parent sample (with ≈ 5.36 million objects) are expected to pass the p_{resnet} threshold, which are still manageable in terms of visual inspections. For Classifier-1, the threshold is $p_{\text{resnet}} = 0.9731$ and the corresponding TPR is 0.85. For Classifier-2, the threshold is $p_{\text{resnet}} = 0.987$ and the corresponding TPR is 0.60.

5. Strong Lens Candidates in the HSC

5.1. Candidates from Classifier-1

Applying Classifier-1 to our parent sample returns 5,468 unique objects with $p_{\text{resnet}} \geq 0.9731$. This fraction, i.e. $5,468/5,356,628 = 0.00102$, is consistent with the FPR of 10^{-3} inferred from the test set, which suggests that Classifier-1 is not over-fitted. Those 5,468 objects are considered as strong-lens candidates and passed to visual inspections. The photometric redshift and i -band magnitude distributions for the candidate lens galaxies are shown in Figure 4 (red contours).

For the visual inspections, author Y. S. performed an initial check of all the 5,468 objects and removed 1,479 obvious non-lenses, which are mostly spiral galaxies, clearly isolated objects, and artefacts. Five authors (Y. S., R. C., S. S., S. H. S., and S. T.) then independently inspected the colour composite cutouts ($10'' \times 10''$, constructed from gri filters) with different scaling schemes and contrasts for the remaining 3,989 objects and as-

signed an integer score between 0 and 3 to each system following the criteria adopted in Sonnenfeld et al. (2018), Cañameras et al. (2020), and Cañameras et al. (2021). Specifically, score 3 corresponds to definite lenses with clear multiple images in configurations that a lens model can easily reproduce. Score 2 corresponds to probable lenses that have extended and distorted arcs but no clear signs of counter-images and/or would require a lens model to explain the configuration. Score 1 corresponds to possible lenses with single arcs far away from the central galaxy, and score 0 corresponds to non-lenses including spirals, ring galaxies, and everything else. The standard deviation of the scores from the five graders was computed for every system. We notice that objects with high standard deviations usually show ambiguous arc-like features, which can be interpreted as either lensed background sources or spiral arms of the central galaxies. 531 objects with standard deviations above 0.75 were therefore regraded by the five graders.

The visual-inspection scores were averaged over the five graders. 92 systems with average scores $\langle S \rangle \geq 2.5$ are considered as grade-A strong-lens candidates and 468 systems with $1.5 \leq \langle S \rangle < 2.5$ are considered as grade-B strong-lens candidates. Among the 5,468 systems that got inspected, there are 78 grade-A/B SuGOHI galaxy-galaxy strong-lens candidates (again excluding candidates from Sonnenfeld et al. (2020) for the sake of simplicity), and 71 of them have average scores $\langle S \rangle \geq 1.5$. The recall of our visual-inspection procedure is therefore estimated to be 91%. The photometric redshift and i -band magnitude distributions for the lens galaxies in the 560 grade-A/B candidates are also shown in Figure 4. Among them, 216 (39%) grade-A/B candidates contain lens galaxies at $z_d^{\text{phot}} \geq 0.6$ and 22 (4%) grade-A/B candidates contain lens galaxies at $z_d^{\text{phot}} \geq 0.8$.

5.2. Candidates from Classifier-2

Applying Classifier-2 to our parent sample returns 6,119 unique objects with $p_{\text{resnet}} \geq 0.987$, which is also consistent with the expectation of $\text{FPR}=10^{-3}$.

Among the 6,119 candidates, 804 were also found by Classifier-1, so their visual-inspection scores were directly set to values from the previous round. Author Y. S. inspected the remaining 5,315 candidates and removed 4,175 candidates that appeared to be non-lenses. The remaining 1,140 candidates were inspected by the same five graders independently. 233 candidates with standard deviations above 0.75 and average score above 1.0 were re-graded. Afterwards, the average visual-inspection scores were computed. In total, Classifier-2 discovers 69 grade-A ($\langle S \rangle \geq 2.5$) and 337 grade-B ($1.5 \leq \langle S \rangle < 2.5$) strong-lens candidates. Among the 6,119 systems that got inspected, there are 55 grade-A/B SuGOHI galaxy-galaxy strong-lens candidates, and 51 of them have average scores $\langle S \rangle \geq 1.5$. It confirms once again that the recall of our visual-inspection procedure is $\approx 92\%$.

Compared to Classifier-1, all 6119 candidates and the 406 grade-A/B candidates found by Classifier-2 tend to contain a higher fraction of higher-redshift and fainter lens galaxies (Figure 4). There are 236 (58%) grade-A/B candidates with lens galaxies at $z_d^{\text{phot}} \geq 0.6$ and 32 (8%) grade-A/B candidates with lens galaxies at $z_d^{\text{phot}} \geq 0.8$. Further considering the lower TPR of Classifier-2, the results suggest that Classifier-2 is more effective in finding strong-lens systems with faint/high-redshift lens galaxies. The reported photometric redshift for one grade-B strong-lens candidate, HSC J100400+010320, is zero, which is

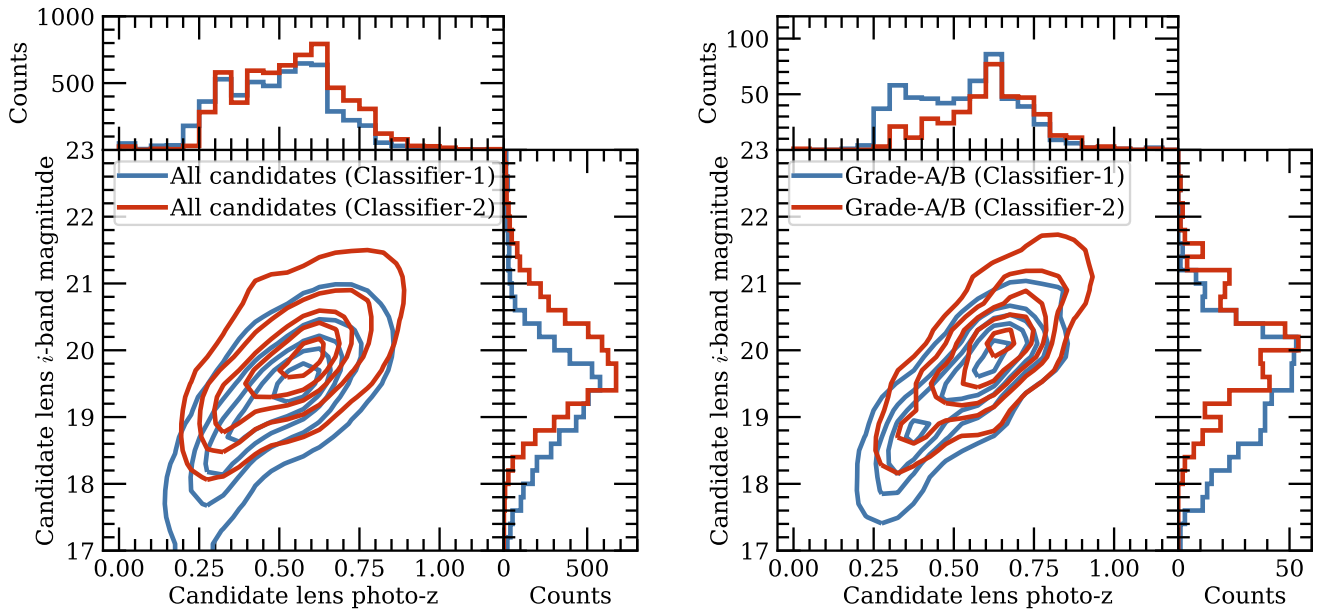


Fig. 4: Distributions of photometric redshift and i -band magnitude of the lens galaxies in strong-lens candidates found by our two classifiers (left) and the subsamples that are classified as grade-A or grade-B after visual inspections (right). In both panels, the contours correspond to 10th, 30th, 50th, 70th and 90th percentiles of the individual dataset.

believed to be a catastrophic outlier in the photometric redshift estimation after checking its image.

5.3. The combined sample

Combining candidates from the two classifiers, we discover in total 105 grade-A and 630 grade-B strong-lens candidates, of which 56 grade-A and 175 grade-B candidates are found by both classifiers. Crossmatching with the known strong lens compilation suggests that 9 grade-A and 268 grade-B candidates are new discoveries. Figure 5 shows the colour composite images of the 105 grade-A candidates, with the new discoveries indicated by a red background beneath the system name. Lists of all grade-A and grade-B candidates are presented in Table B.1 and Table B.2, and colour composite images of all grade-B candidates are shown in Figure B.1.

There is considerable diversity in the lens and source populations in the discovered grade-A/B strong-lens candidates. The majority of them consist of a single elliptical lens galaxy surrounded by blue, extended lensing-like features, indicating star-forming source galaxies. Nonetheless, some candidates contain disk lens galaxies, for example, HSC J015758–061426, HSC J092829–004513, and HSC J144228+002105. Some candidates show orange/red lensing-like features from source galaxies with overall old stellar populations and/or noticeable dust attenuation, for example, HSC J021134–023752, HSC J093707+002731, and HSC J155957+441543. Some candidates show multiple lensed background sources as being compact, for example, HSC J115252+004733, HSC J122102+001853, and HSC J224842+052217. In addition, there are also some group-scale strong-lens candidates, for example, HSC J015824–004001, HSC J022410–033605, and HSC J222609+004141.

Nearly half of the discovered grade-A/B strong-lens candidates, i.e. 331/735, contain lens galaxies with $z_d^{\text{phot}} \geq 0.6$, of

which 4 grade-A and 129 grade-B candidates are new discoveries. 42 candidates contain lens galaxies with $z_d^{\text{phot}} \geq 0.8$, of which 1 grade-A and 12 grade-B candidates are new discoveries. According to Figure 4, the candidate lens galaxies cover a broad magnitude range of 1–2 mag at a fixed redshift, indicating a span of 0.4–0.8 dex in lens galaxy mass.

5.4. Auxiliary Spectroscopic Data

We crossmatch our 735 grade-A/B strong-lens candidates with spectroscopic catalogues from SDSS-I (Abazajian et al. 2009), SDSS-III (Alam et al. 2015), SDSS-IV (Ahumada et al. 2020), the Master Lens Database¹, and the SuGOHI project website² using a matching radius of $1''$, and obtain spectroscopic redshifts for lens galaxies in 333 candidates and spectroscopic redshifts for source galaxies in 24 candidates. The HSC photometric redshifts for the 333 candidate lens galaxies are in excellent agreement with the corresponding spectroscopic redshifts. The differences between the photometric redshifts and spectroscopic redshifts have a mean of -0.009 and standard deviation of 0.06 in the redshift range of 0.23–0.86. This agreement suggests that the photometric redshift estimation for candidate lens galaxies in our sample is barely affected by the presence of surrounding potential lensed features. This is understandable as our visual inspection process preferentially picks out candidates that exhibit clear separations between the central galaxies and potential lensed features. Moreover, CModel photometry, instead of aperture photometry, is used for the photometric redshift estimation (Tanaka et al. 2018), in which substantial deblending from surrounding features is already involved. It also indicates that the photometric redshifts for the remaining candidate lens galaxies are likely reliable.



Fig. 5: Colour composite images ($10'' \times 10''$) of the 105 grade-A strong-lens candidates discovered by this work. Candidates with red background beneath the system name are new discoveries.

6. Notes on individual systems

We carry out visual inspections of the publicly available spectra of the 333 candidates identified in the previous Section and find six cases where prominent emission lines not consistent with the redshift of the candidate lens galaxies are detected, suggesting superpositions of two objects along the same line of sight. We discuss those cases one by one in this Section.

HSC J020241–064611 This is a grade-B candidate according to our visual inspection. Two purple, arc-like features are found on the north and south sides of an orange, elliptical galaxy with a separation of $\approx 1''.8$ (Figure B.1). A fiber-fed ($2''$ in diameter) spectrum from SDSS-III is available, which shows a high S/N emission line at 4557.2\AA on top of a $z = 0.5020$ early-type galaxy spectrum (Figure 6). This line is obviously not coincident with any typical emission line at $z = 0.5020$. Shu et al. (2016a) interpreted this line as Ly α emission from a Ly α emitter (LAE) at

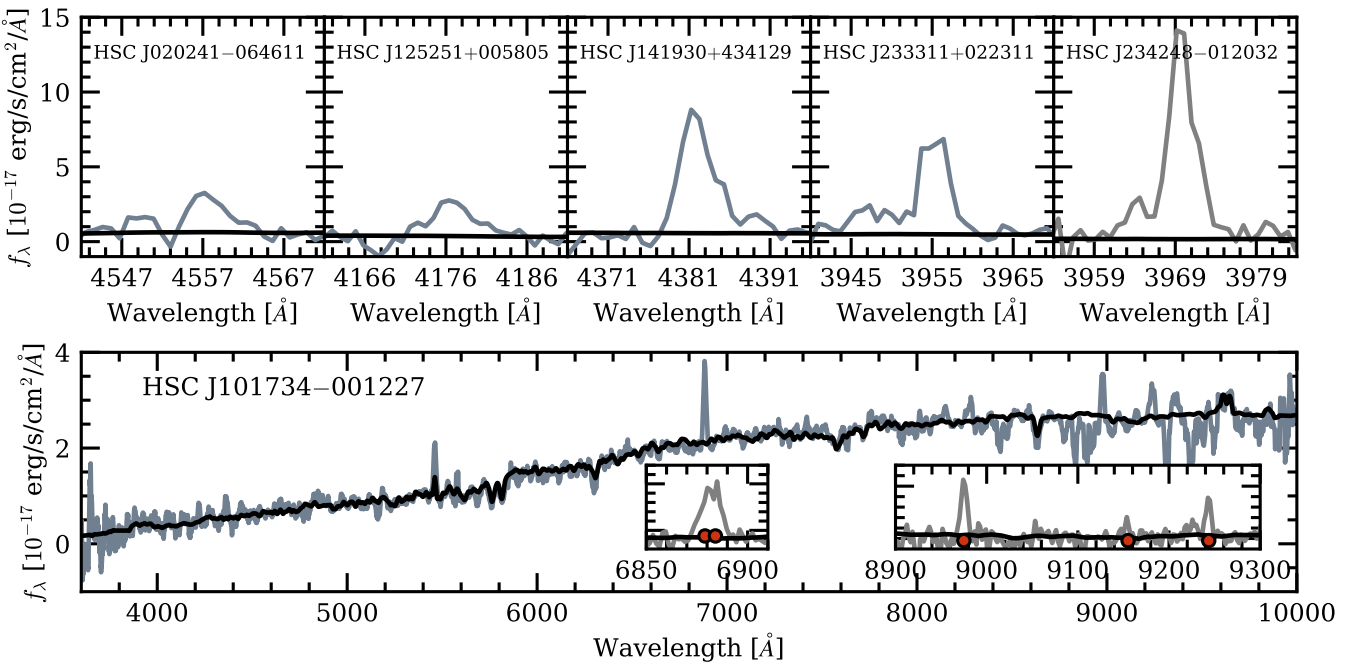


Fig. 6: SDSS spectra of the six strong-lens candidates with evidence for higher-redshift emission lines. In each panel, the grey line represents the observed spectrum and the black line represents the SDSS-provided best-fit model spectrum (for only the foreground lens galaxy). The top row shows 30Å windows centred on the detected emission line for HSC J020241-064611, HSC J125251+005805, HSC J141930+434129, HSC J233311+022311, and HSC J234248-012032, and the bottom row shows the full optical spectrum for HSC J101734-001227. Several emission lines not associated with the redshift of the foreground galaxy (i.e. $z = 0.4647$) are shown in the zoomed-in insets of the bottom panel. They are found to be coincident with the locations of [OII] doublet, H β , [OIII] 4960, and [OIII] 5008 at $z = 0.8457$.

$z = 2.7477$, and considered this system as a galaxy-LAE strong-lens candidate. This system was also classified, based on HSC data, as a grade-B candidate by Sonnenfeld et al. (2018), who resolved the two arc-like features after subtracting the foreground galaxy light. Combining imaging and spectroscopic evidence, we speculate that the two arc-like features are lensed images of a $z = 2.7477$ LAE. The SDSS-measured central velocity dispersion for the foreground galaxy is $156 \pm 25 \text{ km s}^{-1}$ ³, which corresponds to an Einstein radius of $\approx 0''.48 \pm 0''.15$ for a source at $z = 2.7477$ and a lens at $z = 0.5020$ with an isothermal total-mass profile. The estimated Einstein radius is $\approx 2.8\sigma$ lower than what is suggested from the image separation.

HSC J101734-001227 This is a grade-B candidate according to our visual inspection and was also classified as a grade-B by C21. A golden, elongated arc is located $\approx 1''.6$ west of a yellow, elliptical galaxy, and there seems to be some hint for a counter image very close to the elliptical galaxy (Figure B.1). A fiber-fed (2'' in diameter) spectrum from SDSS-III is available. The SDSS best-fit model suggests a redshift of 0.8457, which is primarily driven by several strong emission lines being coincident with [OII] doublet, H β , [OIII] 4960, and [OIII] 5008 at

$z = 0.8457$. Nevertheless, it is noticed that some emission and absorption features in the spectrum cannot be explained by the best-fit model. Interestingly, we find that the second-best fit provided by SDSS can well reproduce those emission and absorption features using galaxy templates at $z = 0.4647$ (Figure 6). It hence becomes clear that this particular line of sight contains two galaxies, one at $z = 0.4647$ and the other at $z = 0.8457$. Unfortunately we cannot estimate the Einstein radius because the SDSS-reported velocity dispersion is 850 km s^{-1} , indicating a failure in the measurement. Combining imaging and spectroscopic evidence, we speculate that the potential counter image and/or the elongated arc on the west are responsible for the detected [OII] doublet, H β , [OIII] 4960, and [OIII] 5008 at $z = 0.8457$.

HSC J125251+005805 This is a grade-B candidate according to our visual inspection. A blue, elongated arc and a similarly blue blob are found on the northeast and southwest sides of a yellow, elliptical galaxy with a separation of $\approx 1''.9$. A fiber-fed (2'' in diameter) spectrum from SDSS-III is available, which shows a high S/N emission line at 4176.4Å on top of a $z = 0.5399$ early-type galaxy spectrum (Figure 6). This line is obviously not coincident with any typical emission line at $z = 0.5399$. Shu et al. (2016a) interpreted this line as Ly α emission from an LAE at $z = 2.4345$, and considered this system as a galaxy-LAE strong-lens candidate. This system was also classified, based on HSC data, as a grade-B candidate by Wong et al. (2018). The SDSS-measured central velocity dispersion for the foreground galaxy is $203 \pm 40 \text{ km s}^{-1}$, which corresponds to an Einstein radius of $\approx 0''.8 \pm 0''.3$ for a source at $z = 2.4345$ and a lens at $z = 0.5399$ with an isothermal total-mass profile. The estimated Einstein radius is in good agreement with the observed image separation. Combining imaging and spectroscopic evidence, we think that

³ Starting from Data Release 9, SDSS provides two types of velocity dispersion. One is VDISP determined by fitting the observed spectrum with a linear combination of 24 eigenspectra. The other can be inferred from VDISP_LNL, which is the velocity-dispersion likelihood function computed by fitting with a linear combination of 5 eigenspectra while marginalising over redshift uncertainties. As discussed in Shu et al. (2012) and Bolton et al. (2012b), velocity dispersions inferred from VDISP_LNL are more robust for SDSS-III galaxies, the spectra of which often have relatively low S/N. We therefore adopt the velocity dispersion inferred from VDISP_LNL in this work.

the blue arc and blob are indeed lensed images (in a cusp configuration) of a $z = 2.4345$ LAE.

HSC J141930+434129 This is a grade-B candidate according to our visual inspection. A blue, elongated arc is located $\approx 1''.5$ southwest of a yellow, elliptical galaxy, but there is no decisive sign for any counter image in the HSC data (Figure B.1). A fiber-fed (2'' in diameter) spectrum from SDSS-IV is available, which shows a high S/N emission line at 4381.3Å on top of a $z = 0.5447$ early-type galaxy spectrum (Figure 6). We have verified that the detected line is present in the 1-D spectra from three individual sub-exposures. This line is obviously not coincident with any typical emission line at $z = 0.5447$. It is also unlikely to be a low-redshift [OII] doublet, because no other strong emission is detected at wavelength positions that would correspond to H β , [OIII], and H α . We hence interpret this line as Ly α emission at $z = 2.6030$. The SDSS-measured central velocity dispersion for the foreground galaxy is 200 ± 40 km s $^{-1}$, which corresponds to an Einstein radius of $\approx 0''.8 \pm 0''.3$ for a source at $z = 2.6030$ and a lens at $z = 0.5447$ with an isothermal total-mass profile. Combining imaging and spectroscopic evidence, we speculate that the detected Ly α emission is primarily from the blue arc on the southwest (due to scattering). If there is indeed a faint counter image close to the foreground galaxy, which is consistent with the Einstein radius estimation, it would also contribute to the detected Ly α emission.

HSC J233311+022311 This is a grade-B candidate according to our visual inspection. Two tangentially elongated blue blobs are located $\approx 1''.3$ southeast of a yellow, elliptical galaxy, and there is no sign for any counter image in the HSC data (Figure B.1). A fiber-fed (2'' in diameter) spectrum from SDSS-III is available, which shows a strong emission line at 3955.5Å on top of a $z = 0.4716$ early-type galaxy spectrum (Figure 6). This line is obviously not coincident with any typical emission line at $z = 0.4716$. Shu et al. (2016a) interpreted this line as Ly α emission from an LAE at $z = 2.2529$, and considered this system as a galaxy-LAE strong-lens candidate. This system was also classified, based on HSC data, as a grade-B candidate by Wong et al. (2018). The SDSS-measured central velocity dispersion for the foreground galaxy is 272 ± 55 km s $^{-1}$, which corresponds to an Einstein radius of $\approx 1''.4 \pm 0''.6$ for a source at $z = 2.2529$ and a lens at $z = 0.4716$ with an isothermal total-mass profile. Combining imaging and spectroscopic evidence, we speculate that the detected Ly α emission is primarily from the two blue blobs on the southeast. If there is indeed a faint counter image close to the foreground galaxy, which is broadly consistent with the Einstein radius estimation, it would also contribute to the detected Ly α emission.

HSC J234248–012032 This is a grade-B candidate according to our visual inspection. A blue, elongated arc and a similarly blue blob are found on the northwest and southeast sides of a yellow, elliptical galaxy with a separation of $\approx 2''.1$. A fiber-fed (2'' in diameter) spectrum from SDSS-III is available, which shows a high S/N emission line at 3970.1Å on top of a $z = 0.5270$ early-type galaxy spectrum (Figure 6). This line is obviously not coincident with any typical emission line at $z = 0.5270$. Shu et al. (2016a) interpreted this line as Ly α emission from an LAE at $z = 2.2649$, and considered this system as a galaxy-LAE strong-lens candidate. The SDSS-measured central velocity dispersion for the foreground galaxy is 271 ± 44 km s $^{-1}$, which corresponds to an Einstein radius of $\approx 1''.4 \pm 0''.4$ for a source at $z = 2.2649$ and a lens at $z = 0.5270$ with an isothermal total-mass profile. The estimated Einstein radius is in good agreement with the observed image separation. Combining imaging and spectroscopic

evidence, we speculate that the blue arc and blob are indeed lensed images (in a cusp configuration) of a $z = 2.2649$ LAE.

7. Discussions

As already mentioned in Section 5, Classifier-2 is found to be more effective than Classifier-1 in discovering strong-lens systems with high-redshift/faint lens galaxies, which, essentially, is a result of differences in the training set and pre-processing steps. 60% and 28% of the mock lenses used for Classifier-2 are at redshifts above 0.6 and fainter than $i = 20.5$ mag respectively, while these two fractions are only 24% and 4% for Classifier-1. In addition, the square-root stretch implemented only in Classifier-2 helps to better reveal lensed features in high-redshift lenses, which, by construction, require higher-redshift sources that appear fainter on average than sources in lower-redshift lenses. Interestingly, we find that including the two pre-processing steps (square-root stretch and normalisation) in Classifier-1 or removing them in Classifier-2 leads to worse performance in terms of AUROC. These findings highlight that the outcome of supervised machine learning techniques depends strongly on the training set and pre-processing procedures need to be chosen in accordance with the training set. We have tested training classifiers with *griz*-filter (instead of *gri*) cutouts, but the performance is not as good as the two presented classifiers. More thorough discussions on the impact of the training set will be presented in Cañameras et al. (in prep.) and More et al. (in prep.).

According to the 0.85 TPR for Classifier-1 and $\approx 92\%$ visual-inspection recall, the 560 grade-A/B strong-lens candidates discovered by Classifier-1 suggest that, in our parent sample, there would be 716 strong lenses in total with properties similar to the 92 SuGOHI strong-lens candidates in our test set. Likewise, the 406 grade-A/B strong-lens candidates discovered by Classifier-2 with a TPR of 0.60 suggest a total number of 736 strong lenses. These two predictions agree well with each other, and are also consistent with the 735 grade-A/B strong-lens candidates discovered by the two classifiers combined. From another perspective, 84 of the 92 SuGOHI candidates in our test set are recovered by the two classifiers combined, suggesting an overall recall of 91%. We therefore expect that $\geq 90\%$ of all strong-lens candidates that are in our parent sample and have properties similar to the 92 SuGOHI strong-lens candidates have already been included in our lists of grade-A/B strong-lens candidates.

Collett (2015) made a prediction on the population of detectable galaxy-galaxy strong lenses in several imaging surveys. Although HSC was not considered there, we can use results for the LSST, relevant properties of which (including pixel scale, seeing distribution, and sky-brightness distribution) are similar to HSC, as an approximation. In particular, Collett (2015) forecasted that LSST can detect, over an area of $20,000$ deg 2 , 17,000 galaxy-galaxy strong lenses from the best single-epoch imaging and 39,000 galaxy-galaxy strong lenses from the final full stack of the survey. The nominal depths of LSST single-epoch and full-stack imaging are {25.0, 24.7, 24.0} and {27.4, 27.5, 26.8} in { g , r , i } filters (Ivezić et al. 2019), which nicely bracket the depths of HSC PDR2. It is hence suggested that the total number of detectable galaxy-galaxy strong lenses in HSC PDR2 is between 800 and 1900. In terms of high-redshift strong lenses, the forecast is that there will be between 180 and 190 $z_d > 0.8$ strong lenses. We note that the actual number of detectable strong lenses is very sensitive to the adopted S/N threshold. Collett (2015) considered a lens system to be detectable if the total S/N, SN_{TOT} , of the lensed features is 20 or higher in at least one band (along with three other conditions). If requiring

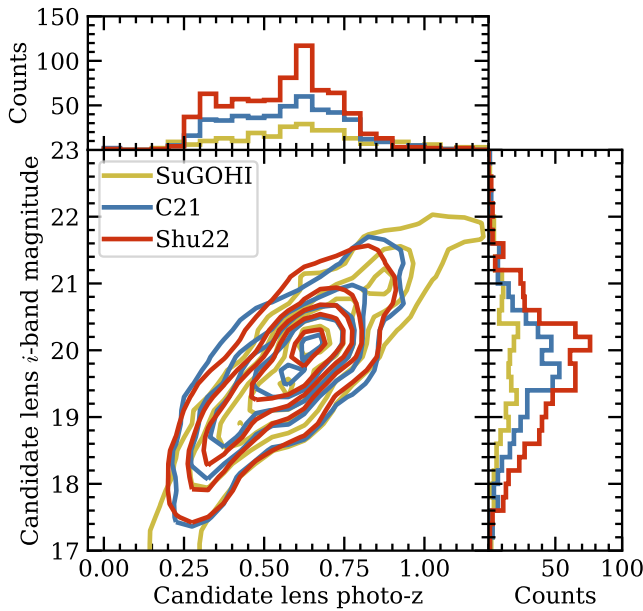


Fig. 7: Distributions of photometric redshift and i -band magnitude of the lens galaxies in galaxy-scale strong-lens candidates from the SuGOHI project (yellow), C21 (blue), and this work (red). The contours correspond to 10th, 30th, 50th, 70th and 90th percentiles of the individual samples. To make a fair comparison, we use `photoz_best` from the `pdr2_wide.photoz_mizuki` table for SuGOHI lens galaxies instead of the photometric redshifts provided by the SuGOHI project website².

$\text{SN}_{\text{TOT}} > 30$, the forecasts for the total number of strong lenses and $z_d > 0.8$ strong lenses in HSC PDR2 drop to 300–1200 and 80–110. On the other hand, Collett (2015) pointed out that their LSST forecasts are likely underestimated due to poorly constrained redshift and size distributions of source galaxies used in their simulation, especially on the faint end. The uncertainties are estimated to be on the level of $\sim 10\%$. It is unclear what fraction of the detectable strong lenses simulated in Collett (2015) will pass our selection criteria in Section 2. Nevertheless, we believe that the vast majority of our grade-A/B strong-lens candidates have SN_{TOT} substantially higher than 20 according to Figure 5 and Figure B.1, and our single set of 735 grade-A/B strong-lens candidates (including 42 at $z_d^{\text{phot}} > 0.8$) represents $\gtrsim 50\%$ of all detectable strong lenses in HSC PDR2.

Prior to this work, there were two other projects that searched systematically for strong lenses in the HSC data. One of them is the SuGOHI project and the other is a project also done by us, i.e. C21. The SuGOHI project makes use of several different methods for lens search including automated algorithms (e.g., Sonnenfeld et al. 2018; Chan et al. 2020) and crowdsourcing (e.g., Sonnenfeld et al. 2020). C21 makes use of a resnet, similar to this work. Time-wise, the resnets used in C21 and this work are many orders of magnitude faster than the automated algorithms and crowdsourcing used in the SuGOHI project. Classifications of the 5.3 million objects in this work took ≈ 100 minutes, or $\approx 50,000$ objects per minute. The classification speed of the methods used in the SuGOHI project is on the order of ~ 10 s per object (K. Wong, private communication).

A more fundamental distinction between the three projects is on the parent sample. The parent sample of this work con-

tains galaxies (or more precisely speaking, extended objects) in the Wide layer of HSC PDR2 that satisfy certain magnitude and colour cuts defined in Section 2 (along with some quality flags). The parent sample in C21 is 62.5 million galaxies in the Wide layer of HSC PDR2 with i -band Kron radius larger than $0.8'$. The parent samples in the SuGOHI project are more heterogeneous and selected not only from the Wide layer but also HSC Deep and UltraDeep fields. In particular, the parent samples in Sonnenfeld et al. (2018), Wong et al. (2018), and Chan et al. (2020) are $\approx 500,000$ luminous red galaxies selected for spectroscopic observations in SDSS-III. The parent sample in Sonnenfeld et al. (2020) is $\approx 300,000$ galaxies with photometric redshifts between 0.2 and 1.2 and stellar mass above $10^{11.2} M_\odot$. In our parent sample, 3,493,859 (65.2%) objects have i -band Kron radius smaller than $0.8'$ and 4,957,066 (92.5%) objects do not satisfy either of the two requirements in the SuGOHI project. As a result, approximately 3.4 million objects in our parent sample had not been classified by either the SuGOHI project or C21.

The SuGOHI project has discovered 497 grade-A/B strong-lens candidates, of which 248 are classified as galaxy-scale systems. For the following comparisons, galaxy-scale candidates from Sonnenfeld et al. (2020) are also included in this SuGOHI galaxy-scale sample, although some of them are actually cluster- or group-scale systems as pointed out in Section 2. C21 has discovered 467 grade-A/B strong-lens candidates, almost all of which are galaxy-scale systems. Similarly, almost all of the 735 grade-A/B strong-lens candidates discovered by this work are galaxy-scale systems. There are 132 candidates in common between this work and the SuGOHI project, and 302 candidates in common between this work and C21. Combining these three samples results in 1,002 unique galaxy-scale strong-lens candidates, and 395 of the 735 (54%) grade-A/B strong-lens candidates in this work had not been discovered by the other two projects. Candidates in C21 and this work cover similar ranges in photometric redshift and i -band magnitude of the lens galaxies, while the SuGOHI galaxy-scale sample contains a higher fraction of candidates with lens photometric redshifts above ≈ 0.9 (Figure 7). In terms of numbers, 25 candidates in the SuGOHI galaxy-scale sample, 13 candidates in C21, and 11 candidates in our sample have lens photometric redshifts above ≈ 0.9 . Nevertheless, we find that 13 of the 25 $z_d^{\text{phot}} > 0.9$ SuGOHI galaxy-scale candidates and 8 of the 13 $z_d^{\text{phot}} > 0.9$ C21 candidates do not fulfil our colour selection criteria defined in Section 2 (criteria 13–14) and are not included in our parent sample in the first place. Those candidates generally have bluer $g - i$ colours as a result of the contamination from the lensed features, especially in the g -band.

8. Conclusions

In this work, we carry out a search for strong-lens systems consisting of high-redshift lens galaxies in the Wide layer data from HSC-SSP PDR2 with a sky coverage of $\approx 960 \text{ deg}^2$. We first apply several colour and magnitude cuts to reduce the sample size in HSC PDR2 from ≈ 80 million galaxies to ≈ 5.4 million galaxies that are presumably at high redshifts. To further efficiently classify those galaxies, i.e. our parent sample, we construct two strong-lens classifiers based on a deep residual network pre-built in the CMU DeepLens package. The two classifiers, Classifier-1 and Classifier-2, differ mainly in the training set and pre-processing procedures. After training, the two classifiers achieve AUROC values of 0.993 and 0.985 on a test dataset comprising real strong lenses and non-lenses. Applying each of

the two classifiers to the *gri*-filter cutouts (60 pixels \times 60 pixels, 1 pixel = 0.¹⁷) of the parent sample returns network scores p_{resnet} for individual galaxies in ≈ 100 minutes. Adopting p_{resnet} thresholds that correspond to an FPR of 10^{-3} based on the test set, Classifier-1 and Classifier-2 produce 5,468 and 6,119 unique strong-lens candidates. Five authors independently grade those strong-lens candidates based on visual inspections of the cutouts. According to the average visual-inspection scores, 560 candidates identified by Classifier-1 and 406 candidates identified by Classifier-2 are considered as grade-A/B (i.e. definite/probable) strong-lens candidates.

By combining the two samples, we discover in total 105 grade-A and 630 grade-B strong-lens candidates, which is the single largest set of galaxy-scale strong-lens candidates discovered with HSC data to date. Among them, 9 grade-A and 268 grade-B candidates are new discoveries. This list of 735 candidates is expected to include $\gtrsim 90\%$ of all strong-lens candidates that are in our parent sample and have properties similar to the test set. The candidate lens galaxies span a (photometric) redshift range from 0.2 to 1.0. Nearly half of the discovered candidates (331/735) contain lens galaxies with $z_d^{\text{phot}} \geq 0.6$, and 42 candidates contain lens galaxies with $z_d^{\text{phot}} \geq 0.8$. Despite having a lower overall TPR, Classifier-2 discovers a significantly higher fraction of high-redshift ($z_d^{\text{phot}} \geq 0.6$) lens galaxies compared to Classifier-1, which we attribute to differences in the training set and pre-processing procedures.

We obtain spectroscopic redshifts for lens galaxies in 333 candidates and spectroscopic redshifts for source galaxies in 24 candidates by crossmatching our candidates with spectroscopic catalogues in the literature. We find an excellent agreement between the HSC-reported photometric redshifts and the corresponding spectroscopic redshifts for the 333 candidate lens galaxies, indicating that the photometric redshifts for the remaining candidate lens galaxies are likely reliable. In addition, we notice high S/N emission lines in publicly-available spectra of six candidates that are presumably from redshifts higher than those of the foreground galaxies. It is worthwhile carrying out follow-up observations to determine the nature of the detected emission lines and lensing status of the six systems.

We will continue applying our classifiers to future HSC data releases to discover more strong-lens systems. Meanwhile, we will obtain follow-up spectroscopy to confirm the best-quality high-redshift strong-lens candidates from this search, and turn them into powerful probe for galaxy evolution at $z \gtrsim 0.8$. Our discoveries will also serve as a valuable target list for ongoing and scheduled spectroscopic surveys such as the Dark Energy Spectroscopic Instrument (DESI Collaboration et al. 2016), the Subaru Prime Focus Spectrograph project (Takada et al. 2014), and the Maunakea Spectroscopic Explorer (The MSE Science Team et al. 2019). As demonstrated by this work, resnet-based algorithms are a promising approach for efficiently and effectively uncovering the $\sim 10^5$ strong-lens systems expected in forthcoming wide-field imaging surveys such as LSST, Euclid, and CSS-OS. All kinds of scientific applications enabled by strong lensing are expected to benefit from a larger and more complete population of strong-lens systems.

Acknowledgements. The authors thank Drs. Thomas Collett and Kenneth Wong for helpful discussions. Y. S. acknowledges support from the Max Planck Society and the Alexander von Humboldt Foundation in the framework of the Max Planck-Humboldt Research Award endowed by the Federal Ministry of Education and Research. S. H. S. thanks the Max Planck Society for support through the Max Planck Research Group. This project has received funding from the European Research Council (ERC) under the European Union’s Horizon 2020 research and innovation programme (LENSNOVA; grant agreement No 771776).

This research is supported in part by the Excellence Cluster ORIGINS which is funded by the Deutsche Forschungsgemeinschaft (DFG, German Research Foundation) under Germany’s Excellence Strategy – EXC-2094 – 390783311. A. T. J. is supported by P2MI ITB 2021. The Hyper Suprime-Cam (HSC) collaboration includes the astronomical communities of Japan and Taiwan, and Princeton University. The HSC instrumentation and software were developed by the National Astronomical Observatory of Japan (NAOJ), the Kavli Institute for the Physics and Mathematics of the Universe (Kavli IPMU), the University of Tokyo, the High Energy Accelerator Research Organization (KEK), the Academia Sinica Institute for Astronomy and Astrophysics in Taiwan (ASIAA), and Princeton University. Funding was contributed by the FIRST program from the Japanese Cabinet Office, the Ministry of Education, Culture, Sports, Science and Technology (MEXT), the Japan Society for the Promotion of Science (JSPS), Japan Science and Technology Agency (JST), the Toray Science Foundation, NAOJ, Kavli IPMU, KEK, ASIAA, and Princeton University. This paper makes use of software developed for the Large Synoptic Survey Telescope. We thank the LSST Project for making their code available as free software at <http://dm.lsst.org>. This paper is based [in part] on data collected at the Subaru Telescope and retrieved from the HSC data archive system, which is operated by the Subaru Telescope and Astronomy Data Center (ADC) at National Astronomical Observatory of Japan. Data analysis was in part carried out with the cooperation of Center for Computational Astrophysics (CfCA), National Astronomical Observatory of Japan. The Subaru Telescope is honored and grateful for the opportunity of observing the Universe from Maunakea, which has the cultural, historical and natural significance in Hawaii.

References

- Abazajian, K. N., Adelman-McCarthy, J. K., Agüeros, M. A., et al. 2009, ApJS, 182, 543
- Abbott, T. M. C., Adamów, M., Aguena, M., et al. 2021, ApJS, 255, 20
- Abolfathi, B., Aguado, D. S., Aguilar, G., et al. 2018, ApJS, 235, 42
- Ahumada, R., Prieto, C. A., Almeida, A., et al. 2020, ApJS, 249, 3
- Aihara, H., AlSayyad, Y., Ando, M., et al. 2019, PASJ, 71, 114
- Alam, S., Albareti, F. D., Allende Prieto, C., et al. 2015, ApJS, 219, 12
- Auger, M. W., Treu, T., Gavazzi, R., et al. 2010, ApJ, 721, L163
- Bag, S., Shafieloo, A., Liao, K., & Treu, T. 2021, arXiv e-prints, arXiv:2110.15315
- Bayer, J., Huber, S., Vogl, C., et al. 2021, A&A, 653, A29
- Bolton, A. S., Brownstein, J. R., Kochanek, C. S., et al. 2012a, ApJ, 757, 82
- Bolton, A. S., Burles, S., Koopmans, L. V. E., et al. 2008, ApJ, 682, 964
- Bolton, A. S., Burles, S., Schlegel, D. J., Eisenstein, D. J., & Brinkmann, J. 2004, AJ, 127, 1860
- Bolton, A. S., Schlegel, D. J., Aubourg, É., et al. 2012b, AJ, 144, 144
- Bonvin, V., Courbin, F., Suyu, S. H., et al. 2017, MNRAS, 465, 4914
- Brewer, B. J., Marshall, P. J., Auger, M. W., et al. 2014, MNRAS, 437, 1950
- Browne, I. W. A., Wilkinson, P. N., Jackson, N. J. F., et al. 2003, MNRAS, 341, 13
- Brownstein, J. R., Bolton, A. S., Schlegel, D. J., et al. 2012, ApJ, 744, 41
- Bussmann, R. S., Pérez-Fournon, I., Amber, S., et al. 2013, ApJ, 779, 25
- Cañameras, R., Nesvadba, N. P. H., Kneissl, R., et al. 2017, A&A, 600, L3
- Cañameras, R., Schuldt, S., Shu, Y., et al. 2021, A&A, 653, L6
- Cañameras, R., Schuldt, S., Suyu, S. H., et al. 2020, A&A, 644, A163
- Chan, J. H. H., Suyu, S. H., Sonnenfeld, A., et al. 2020, A&A, 636, A87
- Chao, D. C. Y., Chan, J. H. H., Suyu, S. H., et al. 2020, A&A, 640, A88
- Chao, D. C. Y., Chan, J. H. H., Suyu, S. H., et al. 2021, A&A, 655, A114
- Christensen, L., Richard, J., Hjorth, J., et al. 2012, MNRAS, 427, 1953
- Collett, T. E. 2015, ApJ, 811, 20
- Courbin, F., Faure, C., Djorgovski, S. G., et al. 2012, A&A, 540, A36
- Craig, P., O’Connor, K., Chakrabarti, S., et al. 2021, arXiv e-prints, arXiv:2111.01680
- Dawson, K. S., Schlegel, D. J., Ahn, C. P., et al. 2013, AJ, 145, 10
- DESI Collaboration, Aghamousa, A., Aguilar, J., et al. 2016, arXiv e-prints, arXiv:1611.00036
- Desira, C., Shu, Y., Auger, M. W., et al. 2022, MNRAS, 509, 738
- Diehl, H. T., Buckley-Geer, E. J., Lindgren, K. A., et al. 2017, ApJS, 232, 15
- Ding, X., Liao, K., Birrer, S., et al. 2021, MNRAS, 504, 5621
- Fadely, R. & Keeton, C. R. 2012, MNRAS, 419, 936
- Faure, C., Anguita, T., Alloin, D., et al. 2011, A&A, 529, A72
- Goldstein, D. A. & Nugent, P. E. 2017, ApJ, 834, L5
- Grillo, C., Rosati, P., Suyu, S. H., et al. 2018, ApJ, 860, 94
- He, K., Zhang, X., Ren, S., & Sun, J. 2016, arXiv e-prints, arXiv:1603.05027
- Hezaveh, Y. D., Dalal, N., Marrone, D. P., et al. 2016, ApJ, 823, 37
- Huang, X., Storfer, C., Gu, A., et al. 2021, ApJ, 909, 27
- Huang, X., Storfer, C., Ravi, V., et al. 2020, ApJ, 894, 78
- Huber, S., Suyu, S. H., Ghoshdastidar, D., et al. 2021a, arXiv e-prints, arXiv:2108.02789
- Huber, S., Suyu, S. H., Noebauer, U. M., et al. 2021b, A&A, 646, A110

- Inami, H., Bacon, R., Brinchmann, J., et al. 2017, A&A, 608, A2
- Inoue, K. T., Minezaki, T., Matsushita, S., & Chiba, M. 2016, MNRAS, 457, 2936
- Ivezić, Ž., Kahn, S. M., Tyson, J. A., et al. 2019, ApJ, 873, 111
- Jacobs, C., Collett, T., Glazebrook, K., et al. 2019a, ApJS, 243, 17
- Jacobs, C., Collett, T., Glazebrook, K., et al. 2019b, MNRAS, 484, 5330
- Jacobs, C., Glazebrook, K., Collett, T., More, A., & McCarthy, C. 2017, MNRAS, 471, 167
- Jaelani, A. T., More, A., Oguri, M., et al. 2020, MNRAS, 495, 1291
- Koopmans, L. V. E., Treu, T., Bolton, A. S., Burles, S., & Moustakas, L. A. 2006, ApJ, 649, 599
- Kostrzewa-Rutkowska, Z., Kozłowski, S., Lemon, C., et al. 2018, MNRAS, 476, 663
- Lanusse, F., Ma, Q., Li, N., et al. 2018, MNRAS, 473, 3895
- Laureijs, R., Amiaux, J., Arduini, S., et al. 2011, arXiv e-prints, arXiv:1110.3193
- Lemon, C. A., Auger, M. W., McMahon, R. G., & Ostrovski, F. 2018, MNRAS, 479, 5060
- Li, R., Napolitano, N. R., Spiniello, C., et al. 2021, arXiv e-prints, arXiv:2110.01905
- Li, R., Napolitano, N. R., Tortora, C., et al. 2020, ApJ, 899, 30
- Marques-Chaves, R., Pérez-Fournon, I., Gavazzi, R., et al. 2018, ApJ, 854, 151
- Marques-Chaves, R., Pérez-Fournon, I., Shu, Y., et al. 2020, MNRAS, 492, 1257
- Marques-Chaves, R., Pérez-Fournon, I., Shu, Y., et al. 2017, ApJ, 834, L18
- Metcalf, R. B., Meneghetti, M., Avestruz, C., et al. 2019, A&A, 625, A119
- Millon, M., Galan, A., Courbin, F., et al. 2020, A&A, 639, A101
- More, A., Cabanac, R., More, S., et al. 2012, ApJ, 749, 38
- More, A., Lee, C.-H., Oguri, M., et al. 2017, MNRAS, 465, 2411
- More, A., Verma, A., Marshall, P. J., et al. 2016, MNRAS, 455, 1191
- Nierenberg, A. M., Treu, T., Wright, S. A., Fassnacht, C. D., & Auger, M. W. 2014, MNRAS, 442, 2434
- Oguri, M. & Kawano, Y. 2003, MNRAS, 338, L25
- Oguri, M. & Marshall, P. J. 2010, MNRAS, 405, 2579
- Oldham, L., Auger, M. W., Fassnacht, C. D., et al. 2017, MNRAS, 465, 3185
- Pawase, R. S., Courbin, F., Faure, C., Kokotanekova, R., & Meylan, G. 2014, MNRAS, 439, 3392
- Petrillo, C. E., Tortora, C., Vernardos, G., et al. 2019, MNRAS, 484, 3879
- Planck Collaboration, Aghanim, N., Akrami, Y., et al. 2020, A&A, 641, A6
- Prakash, A., Licquia, T. C., Newman, J. A., et al. 2016, ApJS, 224, 34
- Ratnatunga, K. U., Ostrander, E. J., Griffiths, R. E., & Im, M. 1995, ApJ, 453, L5
- Rojas, K., Savary, E., Clément, B., et al. 2021, arXiv e-prints, arXiv:2109.00014
- Ryczkowski, D., Smith, G. P., Bianconi, M., et al. 2020, MNRAS, 495, 1666
- Savary, E., Rojas, K., Maus, M., et al. 2021, arXiv e-prints, arXiv:2110.11972
- Schuldt, S., Suyu, S. H., Cañameras, R., et al. 2021a, A&A, 651, A55
- Schuldt, S., Suyu, S. H., Meinhardt, T., et al. 2021b, A&A, 646, A126
- Shu, X., Yang, L., Liu, D., et al. 2021a, arXiv e-prints, arXiv:2112.03709
- Shu, Y., Belokurov, V., & Evans, N. W. 2021b, MNRAS, 502, 2912
- Shu, Y., Bolton, A. S., Brownstein, J. R., et al. 2015, ApJ, 803, 71
- Shu, Y., Bolton, A. S., Kochanek, C. S., et al. 2016a, ApJ, 824, 86
- Shu, Y., Bolton, A. S., Mao, S., et al. 2018a, ApJ, 864, 91
- Shu, Y., Bolton, A. S., Mao, S., et al. 2016b, ApJ, 833, 264
- Shu, Y., Bolton, A. S., Moustakas, L. A., et al. 2016c, ApJ, 820, 43
- Shu, Y., Bolton, A. S., Schlegel, D. J., et al. 2012, AJ, 143, 90
- Shu, Y., Brownstein, J. R., Bolton, A. S., et al. 2017, ApJ, 851, 48
- Shu, Y., Koposov, S. E., Evans, N. W., et al. 2019, MNRAS, 489, 4741
- Shu, Y., Marques-Chaves, R., Evans, N. W., & Pérez-Fournon, I. 2018b, MNRAS, 481, L136
- Sonnenfeld, A., Chan, J. H. H., Shu, Y., et al. 2018, PASJ, 70, S29
- Sonnenfeld, A., Gavazzi, R., Suyu, S. H., Treu, T., & Marshall, P. J. 2013, ApJ, 777, 97
- Sonnenfeld, A., Verma, A., More, A., et al. 2020, A&A, 642, A148
- Stark, D. P., Auger, M., Belokurov, V., et al. 2013, MNRAS, 436, 1040
- Stark, D. P., Walth, G., Charlton, S., et al. 2015, MNRAS, 454, 1393
- Stein, G., Blaum, J., Harrington, P., Medan, T., & Lukic, Z. 2021, arXiv e-prints, arXiv:2110.00023
- Suyu, S. H., Auger, M. W., Hilbert, S., et al. 2013, ApJ, 766, 70
- Suyu, S. H., Bonvin, V., Courbin, F., et al. 2017, MNRAS, 468, 2590
- Suyu, S. H. & Halkola, A. 2010, A&A, 524, A94
- Suyu, S. H., Hensel, S. W., McKean, J. P., et al. 2012, ApJ, 750, 10
- Suyu, S. H., Huber, S., Cañameras, R., et al. 2020, A&A, 644, A162
- Suyu, S. H., Marshall, P. J., Auger, M. W., et al. 2010, ApJ, 711, 201
- Takada, M., Ellis, R. S., Chiba, M., et al. 2014, PASJ, 66, R1
- Tanaka, M., Coupon, J., Hsieh, B.-C., et al. 2018, PASJ, 70, S9
- The MSE Science Team, Babusiaux, C., Bergemann, M., et al. 2019, arXiv e-prints, arXiv:1904.04907
- Treu, T. 2010, ARA&A, 48, 87
- Treu, T., Dutton, A. A., Auger, M. W., et al. 2011, MNRAS, 417, 1601
- Treu, T., Koopmans, L. V., Bolton, A. S., Burles, S., & Moustakas, L. A. 2006, ApJ, 640, 662
- Vegetti, S., Koopmans, L. V. E., Bolton, A., Treu, T., & Gavazzi, R. 2010, MNRAS, 408, 1969
- Vegetti, S., Lagattuta, D. J., McKean, J. P., et al. 2012, Nature, 481, 341
- Wojtak, R., Hjorth, J., & Gall, C. 2019, MNRAS, 487, 3342
- Wong, K. C., Keeton, C. R., Williams, K. A., Momcheva, I. G., & Zabludoff, A. I. 2011, ApJ, 726, 84
- Wong, K. C., Sonnenfeld, A., Chan, J. H. H., et al. 2018, ApJ, 867, 107
- Wong, K. C., Suyu, S. H., Chen, G. C. F., et al. 2020, MNRAS, 498, 1420
- Wong, K. C., Tran, K.-V. H., Suyu, S. H., et al. 2014, ApJ, 789, L31
- Zhan, H. 2018, in 42nd COSPAR Scientific Assembly, Vol. 42, E1.16-4-18

Appendix A: Visual-inspection Score Comparisons with C21

Among all the network candidates from C21 and this work, 956 systems are in common and have been assigned visual-inspection scores twice by the same five graders. In this Section, we discuss the variations in the visual-inspection scores for the same systems from round to round, which provides an idea on the robustness of our visual-inspection scores. We note that the visual-inspection processes between this work and C21 are slightly different. In C21, three images with different stretching and normalisation schemes for the same systems were provided to the graders, while four more images with different stretching and normalisation schemes for the same systems were provided in this work.

Inevitably, scores from each grader are not all identical. The biases for individual graders range from -0.18 to 0.12 , and the typical dispersion is ~ 0.7 (Figure A.1). Encouragingly, the average score, which determines the final lens grade, has almost no bias (-0.01). Hence, for systems that have different average scores between this work and C21, our recommendation is to adopt the higher values so that a more complete list of candidates can be obtained.

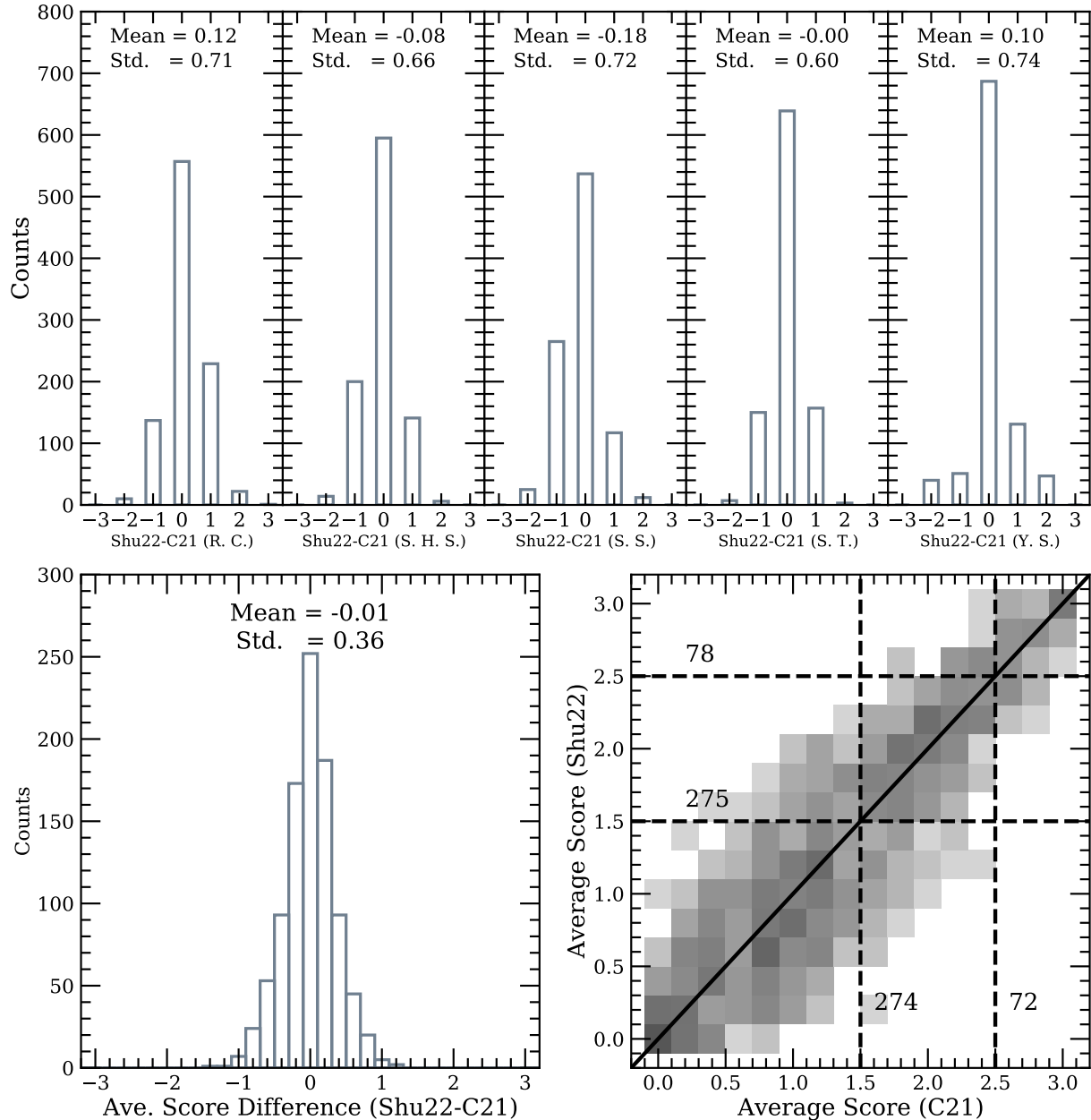


Fig. A.1: Comparisons on visual-inspection scores for the 956 systems that are in common between this work (i.e. Shu22) and C21. The top row shows the distributions of the difference in scores for the five graders (R. C., S. H. S., S. S., S. T., and Y. S.). The mean and standard deviation of the differences for individual graders are given in each sub-panel. The bottom left panel is the distribution of the difference in the average score, which has a mean of -0.01 and standard deviation of 0.36 . The bottom right panel shows the two-dimensional histogram of the average scores in C21 and Shu22. The solid black line is the one-to-one line, and the dashed black lines indicate thresholds that correspond to grade-A/B. According to average scores in C21, 72 are grade As and 274 are grade Bs. According to average scores in this work, 78 are grade As and 275 are grade Bs.

Appendix B: Full lists of grade-A/B lenses

Table B.1: A full list of discovered grade-A strong-lens candidates. Column 1 is the system name. Columns 2 and 3 are right ascension and declination (J2000) of the lens galaxy. Columns 4 and 5 are the i -band CModel magnitude and photometric redshift of the lens galaxy provided by the HSC catalogue. Columns 6 and 7 give the spectroscopic redshifts of the lens and source inferred from auxiliary data. Column 8 indicates the classifier(s) that finds the lens system. Column 9 is the average visual-inspection score of the lens system. Column 10 provides the paper that first discovered the system. Shu22 indicates a completely new discovery. Other relevant references are: Brownstein12: Brownstein et al. (2012); C21: Cañameras et al. (2021); Diehl17: Diehl et al. (2017); Huang20: Huang et al. (2020); Huang21: Huang et al. (2021); Jacobs17: Jacobs et al. (2017); Jacobs19b: Jacobs et al. (2019a); Li20: Li et al. (2020); More12: More et al. (2012); More16: More et al. (2016); More17: More et al. (2017); Petrillo19: Petrillo et al. (2019); Ratnatunga95: Ratnatunga et al. (1995); Shu16: Shu et al. (2016a); Sonnenfeld13: Sonnenfeld et al. (2013); Stark13: Stark et al. (2013); Stein21: Stein et al. (2021); SuGOHI-1: Sonnenfeld et al. (2018); SuGOHI-2: Wong et al. (2018); SuGOHI-4: Chan et al. (2020); SuGOHI-5: Jaelani et al. (2020); SuGOHI-6: Sonnenfeld et al. (2020). And “Guoyou Sun” corresponds to candidates identified by an amateur astronomer, Guoyou Sun, through visual inspections of HSC cutouts (<http://sunguoyou.lamost.org/glc.html>). Systems with \dagger and/or \ddagger are independently discovered by Wong et al. (in prep.) and/or Jaelani et al. (in prep.).

Name	R.A.	Decl.	m_i	z_d^{phot}	z_d^{spec}	$z_{\text{source}}^{\text{spec}}$	Classifier	Score	Reference
HSC J000848+001550	2.20333	0.26412	18.46	0.35 ± 0.03	0.397	—	1	2.6	SuGOHI-5
HSC J012018+001125	20.07557	0.19048	20.14	0.63 ± 0.04	0.599	—	1,2	2.6	C21
HSC J012954+003801	22.47583	0.63363	20.27	0.67 ± 0.05	—	—	1	2.8	C21
HSC J015731–033057	29.38125	−3.51603	20.02	0.68 ± 0.04	0.621	—	1,2	2.8	SuGOHI-1
HSC J015758–061426	29.49429	−6.24057	18.96	0.35 ± 0.03	—	—	1,2	2.6	C21
HSC J015759–054449	29.49622	−5.74709	20.14	0.71 ± 0.04	—	—	1,2	2.6	SuGOHI-6
HSC J015824–004001	29.60321	−0.66702	19.96	0.62 ± 0.04	—	—	1	2.6	Huang20
HSC J015958–050427	29.99278	−5.07437	17.86	0.35 ± 0.03	0.434	—	1	2.8	SuGOHI-6
HSC J020047–034415	30.19811	−3.73761	20.38	0.75 ± 0.03	—	—	1,2	2.6	C21
HSC J020108–041845	30.28334	−4.31267	19.25	0.35 ± 0.05	—	—	1,2	2.8	Shu22
HSC J020141–030946	30.42494	−3.16283	19.18	0.41 ± 0.03	0.362	—	1	2.8	SuGOHI-1
HSC J020338–051901	30.90969	−5.31712	18.70	0.32 ± 0.04	—	—	1,2	3.0	C21
HSC J020832–043315	32.13393	−4.55439	20.99	0.76 ± 0.03	—	—	1,2	2.6	More16
HSC J020929–064312	32.37223	−6.72009	19.21	0.41 ± 0.02	0.407	—	1	3.0	More12
HSC J020955–024442	32.48095	−2.74507	20.08	0.69 ± 0.04	—	—	1,2	2.8	SuGOHI-5
HSC J021134–023752	32.89276	−2.63122	18.70	0.48 ± 0.03	0.573	—	1	2.8	SuGOHI-6
HSC J021411–040502	33.54676	−4.08411	20.15	0.66 ± 0.06	0.609	1.880	1,2	2.6	More12
HSC J022140–021020	35.41724	−2.17223	20.06	0.74 ± 0.03	0.707	—	1,2	2.6	SuGOHI-1
HSC J022222–022211	35.59344	−2.36979	22.16	1.15 ± 0.02	—	—	1	2.6	SuGOHI-5
HSC J022410–033605	36.04321	−3.60151	20.70	0.72 ± 0.04	0.613	—	1	2.6	SuGOHI-1
HSC J023038–015249	37.65891	−1.88028	18.83	0.39 ± 0.03	—	—	1,2	2.6	SuGOHI-6
HSC J023217–021703	38.07240	−2.28439	19.60	0.49 ± 0.04	0.508	—	1,2	2.6	SuGOHI-1
HSC J023249–032326	38.20776	−3.39058	18.37	0.36 ± 0.04	0.450	2.518	1	3.0	Stark13
HSC J023314–024352	38.31201	−2.73124	20.49	0.72 ± 0.04	—	—	2	2.6	SuGOHI-6
HSC J023637–033220	39.15545	−3.53893	18.39	0.27 ± 0.03	0.269	—	1,2	3.0	SuGOHI-1
HSC J084040–003003	130.16871	−0.50089	20.39	0.58 ± 0.05	—	—	1,2	2.6	SuGOHI-6
HSC J085046+003905	132.69420	0.65150	21.57	0.95 ± 0.04	—	—	2	3.0	SuGOHI-6
HSC J085613–014128	134.05727	−1.69121	19.48	0.54 ± 0.04	—	—	1,2	2.6	C21
HSC J090241+025318	135.67122	2.88837	20.29	0.64 ± 0.06	—	—	1	2.6	SuGOHI-6
HSC J090407–005953	136.03306	−0.99807	19.97	0.62 ± 0.04	0.611	2.360	1,2	3.0	More12
HSC J090507–001030	136.28058	−0.17503	18.97	0.50 ± 0.07	0.494	—	1,2	2.6	Petrillo19
HSC J090938+002842	137.41080	0.47847	20.52	0.73 ± 0.04	—	—	1,2	3.0	SuGOHI-6
HSC J091148+041852	137.95383	4.31467	21.12	0.80 ± 0.03	0.861	2.630	2	2.6	SuGOHI-6
HSC J091904+033638	139.76917	3.61072	18.70	0.39 ± 0.05	0.444	—	1,2	3.0	SuGOHI-1
HSC J092544+001702	141.43748	0.28413	20.93	0.84 ± 0.05	—	—	1,2	2.8	SuGOHI-5
HSC J092600–012020	141.50174	−1.33894	20.95	0.81 ± 0.03	—	—	1,2	2.8	C21
HSC J092627+000759 ‡	141.61504	0.13321	21.04	0.64 ± 0.07	—	—	2	2.8	Shu22
HSC J092829–004513	142.12411	−0.75362	18.42	0.42 ± 0.04	0.355	—	1,2	2.8	C21
HSC J093707+002731	144.27941	0.45864	18.22	0.38 ± 0.03	0.412	—	1	2.8	Shu22
HSC J094123+000446	145.34596	0.07964	18.71	0.44 ± 0.05	0.486	—	1,2	2.8	SuGOHI-2
HSC J094327–015453	145.86522	−1.91481	18.63	0.36 ± 0.05	0.450	—	1	2.6	SuGOHI-5
HSC J094348+005926	145.95073	0.99061	19.59	0.43 ± 0.04	—	—	1	3.0	Huang20
HSC J094756+002450	146.98526	0.41414	19.53	0.42 ± 0.11	—	—	1	2.6	Shu22
HSC J095014+023230	147.56176	2.54171	18.57	0.29 ± 0.03	—	—	1,2	2.6	C21

Continued on next page

Table B.1 – continued from previous page

Name	R.A.	Decl.	m_i	z_d	z_d^{spec}	$z_{\text{source}}^{\text{spec}}$	Classifier	Score	Reference
HSC J100703+020834	151.76641	2.14303	18.52	0.34 ± 0.03	—	—	1,2	2.6	C21
HSC J114301–004712	175.75550	−0.78673	17.87	0.27 ± 0.03	—	—	1	2.6	SuGOHI-5
HSC J115011–002019	177.54688	−0.33886	20.09	0.67 ± 0.05	—	—	1,2	2.8	SuGOHI-6
HSC J115252+004733	178.21776	0.79252	19.10	0.46 ± 0.04	0.466	3.760	2	3.0	More17
HSC J115315+012745	178.31498	1.46274	19.28	0.50 ± 0.03	—	—	1,2	2.6	SuGOHI-5
HSC J115329+000018	178.37104	0.00508	19.49	0.43 ± 0.03	—	—	1	2.8	Shu22
HSC J115550+012832 [‡]	178.96039	1.47573	19.44	0.56 ± 0.03	0.576	—	1,2	2.6	Shu22
HSC J120129+001929	180.37158	0.32499	20.25	0.65 ± 0.05	—	—	1	2.6	SuGOHI-6
HSC J121052–011905	182.71866	−1.31814	20.24	0.68 ± 0.04	0.700	2.295	1,2	3.0	SuGOHI-4
HSC J121123–010609	182.84596	−1.10270	19.76	0.58 ± 0.03	—	—	1	2.6	C21
HSC J122102+001853	185.25948	0.31493	21.14	0.92 ± 0.04	—	—	1,2	2.8	C21
HSC J122450–004215	186.20954	−0.70423	17.85	0.36 ± 0.02	0.403	—	1	3.0	Petrillo19
HSC J123421–000926	188.59093	−0.15726	18.89	0.38 ± 0.03	—	—	1,2	3.0	Petrillo19
HSC J123554+005550	188.97573	0.93060	18.06	0.33 ± 0.03	0.416	—	1	2.6	Li20
HSC J123636–003539	189.15056	−0.59418	18.91	0.70 ± 0.03	—	—	1	2.8	Shu22
HSC J124320–004517	190.83655	−0.75494	19.66	0.63 ± 0.04	0.654	—	1,2	3.0	SuGOHI-2
HSC J135710+010325	209.29493	1.05705	19.83	0.77 ± 0.03	—	—	1,2	2.8	Shu22
HSC J135942–012620	209.92846	−1.43917	18.30	0.32 ± 0.04	0.407	—	1	2.6	SuGOHI-5
HSC J140452+005122	211.21787	0.85629	18.17	0.33 ± 0.03	0.398	—	1,2	2.6	SuGOHI-6
HSC J140705–011256	211.77248	−1.21580	18.99	0.64 ± 0.03	0.647	—	1,2	2.8	SuGOHI-1
HSC J140929–011410	212.37375	−1.23633	20.14	0.60 ± 0.04	0.584	2.302	1,2	3.0	SuGOHI-1
HSC J141300–012608	213.25027	−1.43561	20.27	0.75 ± 0.04	0.749	2.666	1,2	2.8	SuGOHI-1
HSC J141735+522646	214.39885	52.44613	20.46	0.79 ± 0.05	0.810	3.400	2	3.0	Ratnatunga95
HSC J142053+005620	215.22340	0.93904	20.51	0.61 ± 0.05	0.615	—	1,2	2.6	SuGOHI-1
HSC J142127+001205	215.36340	0.20149	20.15	0.53 ± 0.03	—	—	1,2	2.8	SuGOHI-5
HSC J142448–005321	216.20415	−0.88935	19.95	0.80 ± 0.03	0.794	1.302	1	3.0	Petrillo19
HSC J142748+000958	216.95147	0.16629	19.89	0.62 ± 0.04	0.589	—	1,2	2.8	SuGOHI-1
HSC J143438+431542	218.65864	43.26171	17.72	0.34 ± 0.02	0.385	—	1	3.0	SuGOHI-5
HSC J143454–005658	218.72664	−0.94964	19.76	0.73 ± 0.03	0.728	—	1,2	3.0	SuGOHI-1
HSC J144101+013344	220.25611	1.56242	20.00	0.73 ± 0.07	—	—	1,2	2.6	Petrillo19
HSC J145217–014714	223.07260	−1.78734	18.84	0.47 ± 0.03	0.507	—	1	2.6	SuGOHI-6
HSC J145236–002142	223.15272	−0.36171	20.36	0.69 ± 0.04	0.733	—	1,2	2.8	SuGOHI-1
HSC J145402+434608	223.51034	43.76905	20.20	0.51 ± 0.15	—	—	2	3.0	C21
HSC J145930+441048	224.87897	44.18021	17.69	0.29 ± 0.03	0.323	—	1	2.8	SuGOHI-5
HSC J150021–004936	225.08752	−0.82689	18.47	0.38 ± 0.04	0.437	—	1	2.6	SuGOHI-6
HSC J155319+431824	238.33075	43.30676	19.35	0.59 ± 0.03	0.629	—	1,2	2.6	SuGOHI-1
HSC J155517+415138	238.82392	41.86074	19.52	0.60 ± 0.04	0.555	—	1,2	2.8	SuGOHI-1
HSC J155732+420623	239.38410	42.10654	19.76	0.46 ± 0.03	—	—	2	2.8	SuGOHI-5
HSC J155826+432830	239.61106	43.47522	18.57	0.38 ± 0.05	0.444	—	1,2	2.6	SuGOHI-1
HSC J155957+441543	239.98977	44.26216	19.75	1.02 ± 0.05	0.598	—	1	2.8	SuGOHI-1
HSC J164151+425917	250.46340	42.98812	19.40	0.60 ± 0.03	0.600	—	1,2	3.0	C21
HSC J220329+020518	330.87094	2.08856	19.56	0.46 ± 0.09	0.400	2.150	2	3.0	More12
HSC J222609+004141	336.53878	0.69498	20.04	0.64 ± 0.04	0.647	—	1,2	3.0	Diehl17
HSC J223353+015721	338.47419	1.95606	18.31	0.25 ± 0.03	—	—	1	2.6	SuGOHI-5
HSC J223733+005015	339.38976	0.83767	19.86	0.63 ± 0.04	0.605	2.143	1,2	2.6	SuGOHI-1
HSC J223934+023506	339.89447	2.58521	21.87	1.11 ± 0.07	—	—	1,2	3.0	SuGOHI-5
HSC J224201+022810	340.50495	2.46958	19.10	0.41 ± 0.05	0.443	—	1	2.6	SuGOHI-1
HSC J224221+001144	340.58993	0.19573	18.85	0.37 ± 0.02	0.385	—	1	3.0	SuGOHI-1
HSC J224842+052217 [‡]	342.17737	5.37159	21.61	0.90 ± 0.09	—	—	2	2.8	Shu22
HSC J224932+031114	342.38647	3.18736	19.05	0.30 ± 0.10	—	—	1,2	2.6	C21
HSC J230521–000211	346.34029	−0.03658	19.46	0.49 ± 0.03	0.492	—	1,2	3.0	SuGOHI-2
HSC J231333–000245	348.38884	−0.04589	20.66	1.43 ± 0.01	—	—	1,2	2.8	Huang21
HSC J231933–010609	349.89018	−1.10275	20.42	0.59 ± 0.05	0.593	—	1,2	2.8	Huang21
HSC J232557–005226	351.48909	−0.87412	20.65	0.79 ± 0.03	—	—	2	2.8	Huang20
HSC J232833+024214	352.13849	2.70399	19.14	0.44 ± 0.03	0.493	—	1	2.6	C21
HSC J233043+015812	352.68165	1.97026	21.37	0.77 ± 0.04	—	—	2	2.6	SuGOHI-5
HSC J233106+000012	352.77706	0.00355	20.07	0.66 ± 0.04	—	—	2	2.6	SuGOHI-5
HSC J233130+003733	352.87700	0.62595	19.77	0.53 ± 0.04	0.552	—	1	3.0	SuGOHI-2
HSC J233146+013845	352.94338	1.64600	19.25	0.46 ± 0.03	0.476	—	1,2	2.8	SuGOHI-2
HSC J233230+003821	353.12887	0.63939	20.20	0.65 ± 0.05	0.623	—	1	2.6	SuGOHI-2
HSC J234018+013036	355.07700	1.51023	19.69	0.58 ± 0.04	0.556	—	1	2.6	C21

Table B.2: A full list of discovered grade-B strong-lens candidates. The columns are the same as in Table B.1

Name	R.A.	Decl.	m_i	z_d^{phot}	z_d^{spec}	$z_{\text{source}}^{\text{spec}}$	Classifier	Score	Reference
HSC J000018+001617	0.07884	0.27158	19.91	0.63 ± 0.04	—	—	2	2.0	Shu22
HSC J000020–002051	0.08681	−0.34750	20.56	0.95 ± 0.05	0.560	—	1	2.2	Shu22
HSC J000106+010329 [‡]	0.27710	1.05827	20.07	0.73 ± 0.03	0.721	—	1,2	2.0	Shu22
HSC J000114+001619	0.31063	0.27214	19.41	0.67 ± 0.05	0.664	—	1	1.6	Shu22
HSC J000327+021020	0.86261	2.17248	20.18	0.72 ± 0.03	—	—	1	1.8	C21
HSC J000507+004518	1.28137	0.75504	18.33	0.89 ± 0.01	—	—	1	1.6	Shu22
HSC J000644+014123	1.68590	1.68996	19.09	0.30 ± 0.09	—	—	1	2.2	SuGOHI-5
HSC J000728+012233	1.86762	1.37603	20.95	0.40 ± 0.07	—	—	1	2.2	Shu22
HSC J001313+002759 [‡]	3.30668	0.46665	20.31	0.54 ± 0.04	—	—	1	1.6	Shu22
HSC J001424+004145	3.60116	0.69590	19.56	0.59 ± 0.03	0.570	—	1	2.2	Jacobs19b
HSC J010615+014436	16.56379	1.74340	19.77	0.64 ± 0.04	0.630	—	1,2	1.8	Shu22
HSC J010636–010009	16.65219	−1.00258	19.46	0.47 ± 0.03	0.506	—	1	1.6	Shu22
HSC J010705+020852	16.77346	2.14793	20.41	0.64 ± 0.04	—	—	1	2.2	C21
HSC J010709–001904	16.78855	−0.31790	20.69	0.72 ± 0.05	—	—	2	1.6	Shu22
HSC J010730+000920 [‡]	16.87787	0.15571	17.73	0.28 ± 0.02	0.297	—	1	2.2	Shu22
HSC J010746+011319 [‡]	16.94317	1.22210	18.83	0.34 ± 0.03	—	—	1	2.0	Shu22
HSC J010757+012833	16.99012	1.47583	19.17	0.38 ± 0.03	—	—	1	1.6	Shu22
HSC J011015+000141	17.56275	0.02829	18.59	0.31 ± 0.04	—	—	1,2	2.2	C21
HSC J011225–002247	18.10737	−0.37974	19.65	0.47 ± 0.03	0.466	—	1,2	2.4	SuGOHI-5
HSC J011304+004955	18.26790	0.83213	19.03	0.60 ± 0.02	0.628	—	1,2	1.6	Shu22
HSC J011600+022831	19.00110	2.47536	20.70	0.82 ± 0.09	—	—	1	2.0	Shu22
HSC J011648–003102	19.20388	−0.51725	19.34	0.62 ± 0.03	—	—	2	1.8	Shu22
HSC J011837+015052 [‡]	19.65590	1.84779	20.38	0.48 ± 0.03	—	—	2	1.8	Shu22
HSC J012105–002251	20.27263	−0.38105	19.24	0.39 ± 0.04	—	—	1	1.8	Shu22
HSC J012402–004559 [‡]	21.01060	−0.76648	19.36	0.53 ± 0.04	0.543	—	1,2	1.8	Shu22
HSC J012558+001713	21.49388	0.28713	19.15	0.41 ± 0.05	—	—	2	2.0	Shu22
HSC J012624–003820	21.60210	−0.63916	19.97	0.53 ± 0.03	—	—	1	1.6	Shu22
HSC J015253–050006	28.22237	−5.00193	22.50	0.83 ± 0.16	—	—	1	1.6	Shu22
HSC J015310–042315 [‡]	28.29412	−4.38766	18.19	0.30 ± 0.04	—	—	1	2.0	Shu22
HSC J015347–042419	28.44935	−4.40554	19.45	0.72 ± 0.03	0.687	—	2	1.8	Shu22
HSC J015453–050020	28.72491	−5.00569	18.81	0.40 ± 0.03	—	—	1,2	2.4	C21
HSC J015521–022804	28.83754	−2.46780	19.38	0.49 ± 0.03	0.483	—	1	1.8	Shu22
HSC J015529–015911	28.87431	−1.98667	19.76	0.73 ± 0.02	0.723	—	1	2.4	C21
HSC J015537–044601	28.90539	−4.76705	19.62	0.72 ± 0.03	0.703	—	1	1.6	Shu22
HSC J015618–010747	29.07554	−1.12974	19.93	0.57 ± 0.04	0.542	1.167	1,2	2.0	SuGOHI-2
HSC J015622–061416	29.09275	−6.23794	18.70	0.40 ± 0.04	—	—	1,2	1.6	Shu22
HSC J015716–051513	29.31859	−5.25379	19.09	0.53 ± 0.03	0.560	—	1	1.8	SuGOHI-5
HSC J015719–050039	29.33267	−5.01099	18.22	0.26 ± 0.03	—	—	1	2.2	SuGOHI-5
HSC J015723–005435	29.34740	−0.90973	21.02	0.53 ± 0.05	—	—	1,2	1.8	Shu22
HSC J015731–021503 [‡]	29.38109	−2.25091	20.68	0.68 ± 0.04	—	—	2	2.2	Shu22
HSC J015750–063601	29.45956	−6.60054	18.59	0.28 ± 0.05	—	—	1	1.6	Shu22
HSC J015756–021810	29.48592	−2.30279	18.06	0.33 ± 0.03	0.372	—	1,2	1.8	SuGOHI-1
HSC J015814–052848	29.55897	−5.48009	21.50	0.72 ± 0.04	—	—	2	1.8	Shu22
HSC J015819–015703	29.58114	−1.95094	18.66	0.32 ± 0.04	0.440	—	1,2	1.8	SuGOHI-1
HSC J015845–003016	29.69003	−0.50455	20.58	0.84 ± 0.06	—	—	2	1.8	Shu22
HSC J015913–052502	29.80747	−5.41750	20.09	0.63 ± 0.03	—	—	1	2.0	SuGOHI-6
HSC J015924–051259	29.85198	−5.21649	21.21	0.67 ± 0.06	—	—	2	2.0	Shu22
HSC J015931–051727	29.87924	−5.29091	20.07	0.74 ± 0.05	—	—	2	1.8	Shu22
HSC J015950–043913 [‡]	29.96230	−4.65385	20.46	0.71 ± 0.08	—	—	1,2	2.0	Shu22
HSC J015955–050357	29.98083	−5.06588	19.51	0.44 ± 0.04	—	—	1,2	2.2	C21
HSC J020020–045256	30.08717	−4.88247	19.82	0.64 ± 0.05	0.640	—	2	1.6	SuGOHI-1
HSC J020211–034645	30.54707	−3.77923	17.44	0.24 ± 0.02	0.286	—	1	2.0	SuGOHI-6
HSC J020241–064611	30.67251	−6.76981	19.05	0.42 ± 0.05	0.502	2.748	1	2.0	Shu16
HSC J020255–023951 [‡]	30.73165	−2.66439	20.62	0.68 ± 0.05	—	—	2	1.8	Shu22
HSC J020321–011647	30.83908	−1.27991	19.73	0.67 ± 0.07	0.603	—	1,2	2.2	SuGOHI-5
HSC J020449–020206	31.20785	−2.03507	20.81	0.81 ± 0.04	—	—	1,2	2.2	SuGOHI-6
HSC J020604–030156	31.52008	−3.03248	19.22	0.41 ± 0.05	—	—	1,2	2.2	C21

Continued on next page

Table B.2 – continued from previous page

Name	R.A.	Decl.	m_i	z_d	z_d^{spec}	$z_{\text{source}}^{\text{spec}}$	Classifier	Score	Reference
HSC J020646–042416	31.69258	−4.40461	19.75	0.56 ± 0.03	—	—	1	2.0	C21
HSC J020810–022018	32.04458	−2.33843	20.12	0.60 ± 0.05	—	—	1,2	2.0	SuGOHI-6
HSC J020832–031623	32.13367	−3.27323	19.49	0.45 ± 0.07	0.435	—	2	1.6	Shu22
HSC J020846–032727	32.19523	−3.45771	19.13	0.57 ± 0.03	0.618	—	1	2.2	SuGOHI-1
HSC J020848–042427	32.20111	−4.40757	20.40	0.76 ± 0.02	—	—	1,2	2.4	More16
HSC J020922–062506	32.34511	−6.41838	19.81	0.60 ± 0.03	0.615	—	1	1.8	Shu22
HSC J020928–012056 [‡]	32.37032	−1.34895	18.74	0.30 ± 0.04	—	—	1,2	1.8	Shu22
HSC J021022–032021	32.59534	−3.33937	19.64	0.62 ± 0.03	0.599	—	1,2	1.8	SuGOHI-6
HSC J021124–031354	32.85130	−3.23194	19.57	0.63 ± 0.04	—	—	1	1.6	SuGOHI-6
HSC J021156–032206	32.98460	−3.36834	20.85	0.79 ± 0.09	—	—	2	1.6	C21
HSC J021209–034840	33.03801	−3.81122	20.60	0.74 ± 0.06	—	—	2	1.6	Shu22
HSC J021341–013636 [‡]	33.42089	−1.61006	20.22	0.60 ± 0.04	—	—	1	1.8	Shu22
HSC J021348–020153	33.45396	−2.03154	20.38	0.71 ± 0.05	—	—	1	1.6	Shu22
HSC J021408–020631	33.53338	−2.10876	22.51	0.77 ± 0.05	—	—	1,2	2.0	SuGOHI-5
HSC J021517–061741 [‡]	33.82219	−6.29484	18.03	0.25 ± 0.02	—	—	1	1.8	Shu22
HSC J021552–004958	33.96715	−0.83295	20.40	0.73 ± 0.05	—	—	1	1.6	Shu22
HSC J021604–060812	34.01698	−6.13684	19.63	0.60 ± 0.03	0.573	—	1,2	1.6	SuGOHI-6
HSC J021633–024826	34.13901	−2.80750	20.19	0.57 ± 0.06	0.610	—	1,2	2.0	SuGOHI-6
HSC J021640–033039	34.16832	−3.51090	20.40	0.66 ± 0.05	—	—	2	1.6	SuGOHI-6
HSC J021645–020835	34.18901	−2.14313	20.19	0.62 ± 0.04	—	—	1	2.2	SuGOHI-6
HSC J021737–051329	34.40481	−5.22486	20.21	0.63 ± 0.04	0.646	1.847	1,2	2.4	Sonnenfeld13
HSC J021749–025713 [‡]	34.45548	−2.95368	19.33	0.43 ± 0.07	—	—	2	1.6	Shu22
HSC J021823–053921	34.59833	−5.65593	20.05	0.69 ± 0.05	0.692	—	1,2	2.0	SuGOHI-5
HSC J021856–062733	34.73367	−6.45940	20.09	0.63 ± 0.04	—	—	1,2	2.0	SuGOHI-6
HSC J021950–055706	34.95969	−5.95184	19.61	0.65 ± 0.05	0.652	—	1	1.6	C21
HSC J022008–034852	35.03568	−3.81461	17.75	0.31 ± 0.02	0.327	—	1	1.8	SuGOHI-6
HSC J022042–022200	35.17671	−2.36680	19.17	0.61 ± 0.03	0.546	—	1	2.0	SuGOHI-1
HSC J022045–032559	35.18956	−3.43329	17.82	0.28 ± 0.03	0.328	—	1	2.0	SuGOHI-5
HSC J022056–063934	35.23580	−6.65955	18.01	0.32 ± 0.03	0.330	—	1	1.6	Sonnenfeld13
HSC J022107–035327 [‡]	35.28067	−3.89095	19.26	0.44 ± 0.04	0.430	—	1,2	1.8	Shu22
HSC J022258–012403 [‡]	35.74328	−1.40099	19.88	0.76 ± 0.02	0.694	—	1	1.8	Shu22
HSC J022302–031050	35.75937	−3.18056	19.52	0.61 ± 0.04	—	—	1,2	1.8	SuGOHI-6
HSC J022315–062906	35.81413	−6.48507	19.38	0.49 ± 0.03	0.507	—	1	2.0	More12
HSC J022355–034137	35.98173	−3.69378	21.44	0.73 ± 0.03	—	—	2	2.0	Shu22
HSC J022422–014946	36.09310	−1.82962	19.07	0.61 ± 0.03	0.587	—	1,2	2.2	SuGOHI-6
HSC J022426–033733	36.11084	−3.62596	19.83	0.61 ± 0.04	0.611	—	2	1.8	SuGOHI-1
HSC J022450–021505	36.20966	−2.25153	20.13	0.72 ± 0.02	0.730	—	1	1.6	SuGOHI-6
HSC J022533–015827	36.38958	−1.97418	18.87	0.37 ± 0.04	0.404	—	1	2.0	Shu22
HSC J022535–030530	36.39967	−3.09182	20.15	0.63 ± 0.05	—	—	2	1.8	Shu22
HSC J022630–043753	36.62818	−4.63156	19.97	0.56 ± 0.03	0.591	—	2	2.0	Shu22
HSC J022648–040610	36.70159	−4.10288	20.26	0.71 ± 0.03	0.766	—	2	2.0	Sonnenfeld13
HSC J022841–061729	37.17214	−6.29141	20.28	0.71 ± 0.04	—	—	2	2.0	SuGOHI-5
HSC J022915–060902	37.31536	−6.15068	20.08	0.62 ± 0.04	—	—	1	2.2	SuGOHI-6
HSC J022930–033830	37.37590	−3.64194	21.17	0.77 ± 0.06	—	—	2	1.6	Shu22
HSC J022930–033836	37.37712	−3.64348	20.08	0.64 ± 0.06	0.670	—	1,2	1.6	SuGOHI-1
HSC J023008–054038	37.53601	−5.67740	20.02	0.48 ± 0.03	0.498	—	1,2	1.8	More16
HSC J023016–024444	37.57047	−2.74578	18.94	0.51 ± 0.04	—	—	1,2	2.0	SuGOHI-6
HSC J023019–044237	37.58131	−4.71046	20.06	0.65 ± 0.04	—	—	1,2	1.8	Shu22
HSC J023103–021050	37.76465	−2.18064	19.93	0.74 ± 0.03	—	—	1,2	2.0	SuGOHI-6
HSC J023124–045120	37.85364	−4.85566	20.57	0.67 ± 0.04	—	—	2	1.6	Shu22
HSC J023145–061313 [‡]	37.94073	−6.22055	18.60	0.28 ± 0.04	—	—	1	2.2	Shu22
HSC J023149–031021	37.95422	−3.17266	19.13	0.59 ± 0.03	0.574	—	1	2.0	SuGOHI-6
HSC J023150–020509	37.96172	−2.08591	19.90	0.77 ± 0.02	—	—	1	2.2	SuGOHI-5
HSC J023218–012104	38.07708	−1.35112	18.67	0.36 ± 0.04	0.392	—	1	1.8	SuGOHI-2
HSC J023244–032927	38.18732	−3.49091	19.59	0.33 ± 0.05	—	—	2	1.6	Shu22
HSC J023248–020651	38.20175	−2.11422	20.29	0.74 ± 0.02	—	—	1	1.6	Shu22
HSC J023255–062123	38.23175	−6.35646	18.89	0.34 ± 0.04	—	—	1,2	2.0	Shu22
HSC J023313–024007	38.30653	−2.66879	19.41	0.48 ± 0.03	—	—	2	1.8	Shu22
HSC J023325–053104	38.35474	−5.51791	18.40	0.26 ± 0.05	0.437	—	1,2	1.8	SuGOHI-6
HSC J023333–031448	38.38791	−3.24680	19.38	0.38 ± 0.03	—	—	1	2.2	Shu22

Continued on next page

Table B.2 – continued from previous page

Name	R.A.	Decl.	m_i	z_d	z_d^{spec}	$z_{\text{source}}^{\text{spec}}$	Classifier	Score	Reference
HSC J023337–055856	38.40810	−5.98246	20.22	0.58 ± 0.05	—	—	1,2	1.8	Shu22
HSC J023340–023611	38.42031	−2.60310	20.96	0.74 ± 0.02	—	—	2	1.6	Shu22
HSC J023438–014153	38.65886	−1.69808	19.03	0.32 ± 0.04	—	—	1	2.2	C21
HSC J023444–033540	38.68424	−3.59457	20.01	0.68 ± 0.04	0.556	—	1,2	2.0	SuGOHI-6
HSC J023521–025000	38.84161	−2.83337	19.71	0.63 ± 0.05	—	—	2	1.8	Shu22
HSC J023522–040543	38.84277	−4.09554	20.37	0.72 ± 0.03	—	—	2	1.6	Shu22
HSC J023524–014128 [‡]	38.85150	−1.69112	19.68	0.45 ± 0.04	—	—	2	2.0	Shu22
HSC J023540–040158	38.91931	−4.03284	18.17	0.35 ± 0.03	0.358	—	1	2.2	SuGOHI-6
HSC J023707–023537	39.28165	−2.59371	19.44	0.63 ± 0.03	0.607	—	1,2	1.8	SuGOHI-1
HSC J023717–061056	39.32131	−6.18223	20.10	0.69 ± 0.04	—	—	1,2	2.2	Shu22
HSC J023718–054755	39.32786	−5.79867	18.93	0.31 ± 0.05	—	—	1,2	1.6	C21
HSC J023746–065715	39.44289	−6.95440	19.71	0.54 ± 0.03	—	—	1	1.8	Shu22
HSC J023759–030658	39.49801	−3.11614	19.45	0.65 ± 0.10	0.476	—	1,2	1.6	SuGOHI-2
HSC J023803–023256	39.51338	−2.54896	18.85	0.40 ± 0.05	—	—	1	2.0	Shu22
HSC J023825–052048	39.60434	−5.34680	19.18	0.44 ± 0.03	—	—	1	1.8	Shu22
HSC J023832–045600	39.63579	−4.93353	18.68	0.43 ± 0.03	0.445	—	1	2.4	SuGOHI-6
HSC J023836–033522 [‡]	39.65278	−3.58964	20.32	0.71 ± 0.04	—	—	2	1.6	Shu22
HSC J024024–061631	40.10002	−6.27539	18.39	0.36 ± 0.03	—	—	1	1.8	Shu22
HSC J083651+003038	129.21623	0.51056	20.81	0.84 ± 0.03	—	—	2	2.0	Shu22
HSC J083655–013430	129.23267	−1.57515	17.67	0.29 ± 0.02	—	—	1	2.2	Petrillo19
HSC J083726+015639	129.35909	1.94428	19.29	0.41 ± 0.02	0.396	—	1	2.4	Petrillo19
HSC J083737–000205	129.40816	−0.03477	20.22	0.58 ± 0.04	—	—	2	1.8	Shu22
HSC J083930+021024	129.87665	2.17351	20.24	0.69 ± 0.05	—	—	1,2	1.8	SuGOHI-5
HSC J083943+004740	129.92931	0.79466	19.19	0.61 ± 0.02	0.621	—	1,2	2.2	SuGOHI-1
HSC J084002–000430	130.00852	−0.07506	19.86	0.49 ± 0.03	—	—	1	2.2	C21
HSC J084148–010000	130.45014	−1.00022	19.58	0.77 ± 0.03	—	—	1,2	2.0	SuGOHI-6
HSC J084211+013835	130.54645	1.64323	17.78	0.27 ± 0.03	—	—	1	2.4	Petrillo19
HSC J084245+004359 [‡]	130.68786	0.73313	20.34	0.64 ± 0.05	—	—	1	2.0	Shu22
HSC J084245–000820	130.68834	−0.13891	18.46	0.37 ± 0.03	0.420	—	1	1.8	SuGOHI-6
HSC J084423–001738	131.09584	−0.29401	20.22	0.73 ± 0.04	—	—	2	2.2	C21
HSC J084442–012321	131.17824	−1.38941	19.50	0.57 ± 0.03	—	—	1,2	2.2	C21
HSC J084536–000456	131.40025	−0.08249	19.83	0.72 ± 0.05	—	—	1,2	2.0	SuGOHI-6
HSC J084549–003029	131.45491	−0.50819	20.02	0.64 ± 0.04	—	—	2	1.6	Shu22
HSC J084626–022212	131.60950	−2.37011	18.84	0.40 ± 0.06	—	—	1,2	2.0	C21
HSC J084632–015416	131.63618	−1.90464	20.15	0.78 ± 0.01	—	—	1	2.0	SuGOHI-5
HSC J084722–013441 [‡]	131.84180	−1.57820	18.75	0.45 ± 0.03	—	—	1	2.0	Shu22
HSC J084915–002421	132.31436	−0.40600	18.69	0.58 ± 0.02	—	—	1	1.8	SuGOHI-6
HSC J084958–005306	132.49541	−0.88508	19.77	0.39 ± 0.09	—	—	2	2.0	SuGOHI-6
HSC J085027+020821	132.61562	2.13939	20.65	0.68 ± 0.04	—	—	1	1.8	Shu22
HSC J085041+013538	132.67471	1.59395	18.86	0.33 ± 0.05	—	—	1	1.6	Shu22
HSC J085132+025832	132.88509	2.97579	19.57	0.58 ± 0.05	0.527	—	2	1.8	SuGOHI-1
HSC J085156+013016	132.98736	1.50459	18.67	0.31 ± 0.03	0.327	—	1	2.2	Petrillo19
HSC J085239–010242	133.16413	−1.04510	21.08	0.53 ± 0.05	—	—	2	1.6	Shu22
HSC J085443+002352	133.67945	0.39781	19.60	0.44 ± 0.04	—	—	1,2	1.6	C21
HSC J085508–013118	133.78483	−1.52173	21.06	0.63 ± 0.05	—	—	2	1.6	Shu22
HSC J085508–004257	133.78490	−0.71590	18.79	0.44 ± 0.05	—	—	2	1.8	C21
HSC J085526+005925	133.85867	0.99039	18.21	0.28 ± 0.03	—	—	1	1.8	Shu22
HSC J085550–001755	133.96161	−0.29864	20.45	0.79 ± 0.02	—	—	2	1.6	SuGOHI-6
HSC J085605–000010	134.02303	−0.00305	19.64	0.64 ± 0.04	—	—	2	1.6	SuGOHI-6
HSC J085720–001148	134.33593	−0.19678	20.12	0.45 ± 0.07	—	—	1	1.6	Shu22
HSC J085855–010208	134.73327	−1.03569	18.81	0.57 ± 0.03	0.467	1.421	1,2	2.0	SuGOHI-1
HSC J085912–014153	134.80133	−1.69818	19.32	0.46 ± 0.03	—	—	2	1.6	Shu22
HSC J085937–010706	134.90678	−1.11859	20.19	0.66 ± 0.04	—	—	2	1.6	Shu22
HSC J085938–010213	134.90886	−1.03702	19.06	0.60 ± 0.03	—	—	2	1.6	SuGOHI-6
HSC J085956+003337	134.98507	0.56043	19.73	0.49 ± 0.03	0.486	—	1	2.2	Shu22
HSC J090047+041700	135.19632	4.28355	18.36	0.30 ± 0.03	—	—	1	1.6	SuGOHI-6
HSC J090315–012125	135.81399	−1.35715	18.88	0.42 ± 0.04	—	—	1	1.6	Shu22
HSC J090333–005829	135.88859	−0.97492	18.75	0.39 ± 0.03	—	—	1,2	2.4	More16
HSC J090502+004423	136.26034	0.73999	20.62	0.74 ± 0.05	—	—	2	1.6	SuGOHI-6
HSC J090508+040902	136.28511	4.15072	19.62	0.52 ± 0.03	0.552	—	1,2	1.8	SuGOHI-6

Continued on next page

Table B.2 – continued from previous page

Name	R.A.	Decl.	m_i	z_d	z_d^{spec}	$z_{\text{source}}^{\text{spec}}$	Classifier	Score	Reference
HSC J090515–010155	136.31396	−1.03203	19.31	0.56 ± 0.03	0.612	—	2	2.0	SuGOHI-6
HSC J090611+011951	136.54602	1.33099	20.49	0.67 ± 0.05	—	—	1	2.4	SuGOHI-6
HSC J090618+003053	136.57885	0.51493	21.03	0.90 ± 0.07	—	—	1,2	2.2	SuGOHI-6
HSC J090658+015449	136.74363	1.91368	20.60	0.89 ± 0.03	—	—	2	1.6	Shu22
HSC J090809–000609	137.04089	−0.10263	20.02	0.75 ± 0.02	—	—	1	1.6	Shu22
HSC J090816–000057	137.07070	−0.01598	20.35	0.58 ± 0.05	—	—	1,2	2.0	C21
HSC J090833+000806	137.14127	0.13506	19.76	0.65 ± 0.04	0.689	—	1,2	2.2	SuGOHI-1
HSC J090903–004120	137.26621	−0.68894	18.39	0.30 ± 0.03	0.300	—	1	1.8	SuGOHI-1
HSC J090911+040518	137.29771	4.08842	20.54	0.79 ± 0.03	—	—	2	2.4	SuGOHI-5
HSC J090929+010030	137.37460	1.00835	22.02	0.73 ± 0.06	—	—	2	1.6	Shu22
HSC J091003+025254	137.51585	2.88170	21.43	0.80 ± 0.04	—	—	2	2.4	C21
HSC J091031+003142	137.63166	0.52856	17.98	0.28 ± 0.03	—	—	1	1.8	SuGOHI-6
HSC J091049–011124 [‡]	137.70777	−1.19015	20.90	0.43 ± 0.17	—	—	2	1.6	Shu22
HSC J091126–004508	137.85847	−0.75241	18.85	0.34 ± 0.06	—	—	1	1.8	Petrillo19
HSC J091227–013701	138.11616	−1.61694	19.62	0.58 ± 0.03	0.602	—	1,2	1.8	SuGOHI-5
HSC J091230+041555	138.12526	4.26549	18.45	0.38 ± 0.05	0.453	—	1	2.0	SuGOHI-5
HSC J091312+035214	138.30374	3.87082	19.34	0.49 ± 0.03	0.456	—	1	1.6	SuGOHI-5
HSC J091328–001320 [‡]	138.36755	−0.22236	20.71	0.55 ± 0.06	—	—	2	2.0	Shu22
HSC J091331+003906	138.37957	0.65171	18.15	0.35 ± 0.03	0.409	—	1	1.6	SuGOHI-1
HSC J091347–010741 [‡]	138.44950	−1.12824	19.95	0.76 ± 0.02	—	—	2	1.8	Shu22
HSC J091351+014131	138.46635	1.69203	19.41	0.48 ± 0.07	—	—	1	2.0	SuGOHI-6
HSC J091544–010329	138.93655	−1.05820	21.06	0.67 ± 0.07	—	—	2	2.0	SuGOHI-5
HSC J091608+034710	139.03552	3.78622	19.24	0.53 ± 0.02	0.531	—	1	2.2	SuGOHI-1
HSC J091740+004438	139.42030	0.74390	18.18	0.31 ± 0.03	—	—	1	1.8	SuGOHI-6
HSC J091821+022318 [‡]	139.59160	2.38843	20.51	0.59 ± 0.04	—	—	2	1.6	Shu22
HSC J092101+035521	140.25647	3.92274	19.79	0.56 ± 0.04	0.472	—	1,2	1.8	SuGOHI-1
HSC J092110–010950	140.29267	−1.16400	20.09	0.60 ± 0.04	—	—	1	2.0	C21
HSC J092120+044430	140.33649	4.74183	19.59	0.59 ± 0.04	—	—	2	2.0	SuGOHI-6
HSC J092121+032010	140.34142	3.33626	18.31	0.28 ± 0.03	0.315	—	1	1.8	C21
HSC J092136+021409	140.40273	2.23595	18.55	0.31 ± 0.04	0.319	—	1	2.2	Petrillo19
HSC J092228+002421	140.61745	0.40609	19.14	0.38 ± 0.04	—	—	1	2.0	C21
HSC J092350+003612	140.95842	0.60359	19.99	0.61 ± 0.04	0.593	—	1	1.8	Shu22
HSC J092411–002850	141.04836	−0.48076	19.79	0.54 ± 0.04	0.541	—	1,2	2.0	SuGOHI-1
HSC J092541–010623	141.42301	−1.10648	19.90	0.40 ± 0.04	0.439	—	1,2	2.4	SuGOHI-1
HSC J092545–005656	141.44005	−0.94902	20.26	0.51 ± 0.05	—	—	1	2.0	Shu22
HSC J092612–000625 [‡]	141.55381	−0.10703	20.40	0.54 ± 0.07	—	—	1	2.2	Shu22
HSC J092627–011626	141.61526	−1.27402	19.80	0.30 ± 0.06	—	—	2	2.0	Shu22
HSC J092645–010114	141.68767	−1.02060	18.12	0.37 ± 0.03	0.366	—	1	1.6	SuGOHI-5
HSC J092724–013551	141.85124	−1.59757	21.23	0.44 ± 0.05	—	—	2	1.6	C21
HSC J092804–002059	142.01799	−0.34973	19.49	0.47 ± 0.10	—	—	2	1.8	Shu22
HSC J092816+000409	142.06918	0.06920	17.57	0.27 ± 0.03	0.321	—	1	1.6	Shu22
HSC J092842+011941	142.17544	1.32812	19.52	0.43 ± 0.04	—	—	2	2.2	C21
HSC J092847–012622 [‡]	142.19935	−1.43945	20.18	0.57 ± 0.04	—	—	2	2.0	Shu22
HSC J092854–000833	142.22781	−0.14270	18.45	0.29 ± 0.04	—	—	1	2.2	Shu22
HSC J092914–002823	142.30953	−0.47306	21.13	0.66 ± 0.09	—	—	2	1.6	Shu22
HSC J092926–000549	142.36140	−0.09708	18.48	0.41 ± 0.04	0.417	—	1	2.4	C21
HSC J092927–015238	142.36609	−1.87729	20.40	0.47 ± 0.03	—	—	2	2.0	C21
HSC J092950–004142	142.45867	−0.69514	20.97	0.70 ± 0.05	—	—	2	1.6	Shu22
HSC J093006+013641	142.52898	1.61141	20.26	0.48 ± 0.05	—	—	2	2.0	Shu22
HSC J093008–000330	142.53480	−0.05836	20.63	0.42 ± 0.02	0.575	—	2	2.0	SuGOHI-2
HSC J093037+002705	142.65821	0.45160	19.71	0.46 ± 0.03	0.636	—	1,2	2.0	Shu22
HSC J093100–003810 [‡]	142.75149	−0.63638	20.78	0.55 ± 0.06	—	—	2	2.0	Shu22
HSC J093152+000028	142.96704	0.00804	19.39	0.50 ± 0.05	—	—	2	1.8	Shu22
HSC J093229–001900	143.12279	−0.31694	19.42	0.59 ± 0.04	—	—	1,2	1.6	Shu22
HSC J093232–015156	143.13610	−1.86570	18.83	0.44 ± 0.04	0.553	—	1	2.2	Shu22
HSC J094235–014732	145.64925	−1.79239	19.10	0.47 ± 0.03	—	—	1	1.6	Shu22
HSC J094722–002327	146.84291	−0.39089	18.90	0.49 ± 0.05	0.454	—	1	1.8	Shu22
HSC J094750–011714 [‡]	146.95889	−1.28730	19.09	0.32 ± 0.04	—	—	1	1.8	Shu22
HSC J095020–001904	147.58558	−0.31803	20.07	0.59 ± 0.04	—	—	1,2	2.0	C21
HSC J095027+014143	147.61604	1.69552	19.90	0.44 ± 0.07	—	—	2	1.8	Shu22

Continued on next page

Table B.2 – continued from previous page

Name	R.A.	Decl.	m_i	z_d	z_d^{spec}	$z_{\text{source}}^{\text{spec}}$	Classifier	Score	Reference
HSC J095428+021458	148.61984	2.24965	19.44	0.60 ± 0.03	0.659	—	1	1.6	Shu22
HSC J095628–001819	149.11702	-0.30549	18.65	0.36 ± 0.04	—	—	1,2	2.2	SuGOHI-5
HSC J095658+033130	149.24409	3.52507	19.89	0.68 ± 0.05	—	—	1,2	2.0	C21
HSC J095824+003654	149.60214	0.61518	19.28	0.39 ± 0.03	—	—	1	1.6	Shu22
HSC J095917+010158	149.82091	1.03305	17.94	0.35 ± 0.04	0.446	—	1	1.8	SuGOHI-5
HSC J095918–015934	149.82626	-1.99296	19.49	0.57 ± 0.04	—	—	1	1.6	Stein21
HSC J100050+013251	150.20943	1.54771	20.59	0.68 ± 0.08	—	—	1,2	2.2	C21
HSC J100120+030736	150.33522	3.12667	19.07	0.51 ± 0.04	0.535	—	1,2	1.6	SuGOHI-2
HSC J100400+010320	151.00014	1.05566	20.30	0.00 ± 0.00	—	—	2	1.8	Shu22
HSC J100610+032310	151.54176	3.38627	19.11	0.55 ± 0.02	0.625	—	1	1.6	Shu22
HSC J100659+024735	151.74700	2.79314	18.84	0.47 ± 0.03	0.482	—	1	1.8	SuGOHI-2
HSC J100702–010735	151.76179	-1.12662	17.83	0.26 ± 0.03	0.301	—	1	2.2	C21
HSC J100713+011447	151.80459	1.24664	20.40	0.73 ± 0.03	—	—	1	2.0	Shu22
HSC J100905+004323	152.27238	0.72324	20.34	0.67 ± 0.05	—	—	2	1.8	Shu22
HSC J100954–012224	152.47859	-1.37338	20.39	0.56 ± 0.07	0.516	—	1	2.2	C21
HSC J101149–010525	152.95594	-1.09041	20.53	0.65 ± 0.05	—	—	1	1.8	Shu22
HSC J101726–003200	154.35906	-0.53337	19.00	0.31 ± 0.05	—	—	1	1.6	Shu22
HSC J101734–001227	154.39195	-0.20758	19.63	0.52 ± 0.05	0.846	—	1	1.8	C21
HSC J101807–000812	154.53075	-0.13676	18.61	0.36 ± 0.03	0.372	—	1	2.2	Huang20
HSC J113537+004442	173.90487	0.74512	18.38	0.37 ± 0.02	0.388	—	1	2.0	Shu22
HSC J113800–004418 [‡]	174.50204	-0.73851	20.03	0.56 ± 0.04	—	—	2	2.0	Shu22
HSC J113825–003655	174.60592	-0.61544	20.04	0.67 ± 0.06	—	—	1	1.6	Shu22
HSC J114042–004335	175.17522	-0.72658	20.40	0.73 ± 0.04	—	—	1,2	2.0	Huang21
HSC J114317+004033	175.82437	0.67603	21.12	0.63 ± 0.05	—	—	2	2.0	SuGOHI-5
HSC J114438–002547	176.16184	-0.42978	20.32	0.70 ± 0.03	0.614	—	1,2	1.6	SuGOHI-5
HSC J114444+001346	176.18677	0.22971	19.49	0.46 ± 0.06	0.468	—	1	1.8	SuGOHI-6
HSC J114705+011911	176.77247	1.31984	21.75	0.75 ± 0.04	—	—	2	1.6	SuGOHI-5
HSC J114758+000953	176.99389	0.16497	20.04	0.62 ± 0.03	—	—	1,2	2.2	SuGOHI-6
HSC J114818–004810	177.07531	-0.80301	20.21	0.74 ± 0.02	—	—	1,2	1.6	Shu22
HSC J114830–010146	177.12790	-1.02958	18.68	0.43 ± 0.03	0.442	—	1	2.2	SuGOHI-1
HSC J114852+000945	177.21789	0.16266	19.86	0.59 ± 0.04	0.589	—	1,2	1.6	SuGOHI-6
HSC J114915–000121	177.31520	-0.02257	19.71	0.53 ± 0.04	—	—	1	1.6	Shu22
HSC J114946–002157 [‡]	177.44370	-0.36609	20.29	0.59 ± 0.04	—	—	2	2.2	Shu22
HSC J115118+010754	177.82741	1.13170	19.85	0.52 ± 0.03	0.539	—	1	2.2	SuGOHI-1
HSC J115203–022542 [‡]	178.01260	-2.42834	19.59	0.53 ± 0.04	0.532	—	1	1.8	Shu22
HSC J115255–011946 [‡]	178.22985	-1.32972	20.06	0.57 ± 0.05	—	—	2	1.6	Shu22
HSC J115319+004943	178.32985	0.82885	19.97	0.73 ± 0.02	0.782	—	2	2.0	Shu22
HSC J115412+011527	178.55236	1.25764	18.62	0.46 ± 0.02	0.399	—	1	2.2	SuGOHI-6
HSC J115434–013246	178.64547	-1.54625	20.09	0.76 ± 0.02	—	—	1	2.2	SuGOHI-5
HSC J115441–020616	178.67192	-2.10456	19.69	0.54 ± 0.04	0.550	—	1	1.6	Shu22
HSC J115529–004255	178.87262	-0.71555	21.05	0.86 ± 0.05	—	—	2	1.8	SuGOHI-6
HSC J115557–001238	178.98894	-0.21072	19.47	0.61 ± 0.04	—	—	1,2	2.2	C21
HSC J115558–014442	178.99397	-1.74517	19.44	0.53 ± 0.03	—	—	1,2	2.4	C21
HSC J115653–003948	179.22093	-0.66350	19.63	0.54 ± 0.04	0.508	—	1,2	2.2	Petrillo19
HSC J115711–013850 [‡]	179.29743	-1.64723	18.96	0.37 ± 0.05	—	—	1	2.0	Shu22
HSC J115713–002422	179.30777	-0.40633	19.80	0.57 ± 0.04	0.581	—	1	2.4	C21
HSC J115815–012718	179.56662	-1.45500	19.72	0.61 ± 0.03	0.674	—	1	1.8	SuGOHI-1
HSC J115823+004920	179.59824	0.82243	19.44	0.71 ± 0.03	0.776	—	1	1.6	Shu22
HSC J115856–020146	179.73736	-2.02966	17.65	0.26 ± 0.03	0.281	—	1	2.4	SuGOHI-6
HSC J115857–000531	179.74060	-0.09217	20.46	0.82 ± 0.06	—	—	1,2	1.8	SuGOHI-6
HSC J120009–014615	180.03943	-1.77109	20.80	0.74 ± 0.02	—	—	2	1.8	Shu22
HSC J120110–003826	180.29214	-0.64073	18.82	0.29 ± 0.05	—	—	1	1.6	Shu22
HSC J120119+002330	180.33222	0.39178	19.92	0.72 ± 0.03	—	—	1,2	1.8	C21
HSC J120121–010402	180.33930	-1.06731	19.64	0.49 ± 0.03	0.510	—	2	2.2	Shu22
HSC J120233–002730	180.64155	-0.45839	18.40	0.34 ± 0.03	—	—	1	1.8	SuGOHI-6
HSC J120257–005559	180.73839	-0.93330	20.35	0.69 ± 0.04	—	—	2	1.8	SuGOHI-6
HSC J120320–013114	180.83700	-1.52058	18.57	0.37 ± 0.03	—	—	1	2.4	C21
HSC J120422–001719	181.09432	-0.28882	19.37	0.45 ± 0.03	—	—	1,2	1.6	Shu22
HSC J120601+005653	181.50798	0.94825	19.55	0.57 ± 0.03	0.559	—	1,2	2.0	SuGOHI-1
HSC J120611–010406	181.54895	-1.06842	21.13	0.45 ± 0.07	—	—	1	2.0	C21

Continued on next page

Table B.2 – continued from previous page

Name	R.A.	Decl.	m_i	z_d	z_d^{spec}	$z_{\text{source}}^{\text{spec}}$	Classifier	Score	Reference
HSC J120620+011845	181.58598	1.31252	19.90	0.58 ± 0.03	—	—	1	1.8	SuGOHI-6
HSC J120623+001507	181.59937	0.25198	19.70	0.54 ± 0.03	0.563	3.120	1,2	2.0	SuGOHI-1
HSC J120701–012745	181.75721	-1.46253	19.07	0.32 ± 0.05	—	—	1	2.0	C21
HSC J120738–014610	181.90998	-1.76945	19.22	0.47 ± 0.03	—	—	1	1.8	Shu22
HSC J120806–012233	182.02748	-1.37590	18.71	0.37 ± 0.03	—	—	1	1.8	SuGOHI-6
HSC J120942–011643 [‡]	182.42758	-1.27880	20.44	0.52 ± 0.04	—	—	2	2.0	Shu22
HSC J121022–011201	182.59520	-1.20052	18.57	0.53 ± 0.03	—	—	1	2.0	SuGOHI-5
HSC J121023+005537	182.59827	0.92705	21.18	0.67 ± 0.06	—	—	2	1.6	Shu22
HSC J121055+012928	182.73234	1.49135	19.06	0.58 ± 0.03	0.585	—	1	1.6	Shu22
HSC J121105–004905	182.77194	-0.81815	19.40	0.56 ± 0.03	0.569	—	1	2.0	SuGOHI-1
HSC J121157+002054	182.98754	0.34834	20.27	0.74 ± 0.03	—	—	1	1.8	SuGOHI-5
HSC J121208–000356	183.03582	-0.06581	20.79	0.76 ± 0.02	—	—	2	1.8	SuGOHI-6
HSC J121400–005208	183.50210	-0.86893	18.76	0.39 ± 0.05	0.441	—	1	1.6	SuGOHI-6
HSC J121844+010805	184.68560	1.13473	20.58	0.67 ± 0.15	—	—	2	2.2	Shu22
HSC J122018+011253 [‡]	185.07897	1.21497	19.61	0.61 ± 0.04	—	—	1	2.0	Shu22
HSC J122048+002146	185.20138	0.36278	19.19	0.39 ± 0.03	0.406	—	1	1.6	SuGOHI-2
HSC J122056+002802	185.23501	0.46743	19.24	0.39 ± 0.03	—	—	1	1.8	Shu22
HSC J122122+005431 [‡]	185.34440	0.90872	20.51	0.72 ± 0.07	—	—	2	1.6	Shu22
HSC J122215–001047	185.56524	-0.17981	20.34	0.74 ± 0.03	0.752	—	2	1.8	Shu22
HSC J122221–012653	185.58783	-1.44829	18.79	0.30 ± 0.04	—	—	1	2.0	Shu22
HSC J122314–002939	185.81143	-0.49432	19.51	0.54 ± 0.03	0.547	—	1,2	1.8	SuGOHI-2
HSC J122336+000019	185.90338	0.00547	20.27	0.68 ± 0.05	—	—	2	1.6	Shu22
HSC J122406–012853	186.02915	-1.48159	20.48	0.68 ± 0.03	—	—	1,2	2.2	Shu22
HSC J122438–004153	186.16095	-0.69809	17.74	0.33 ± 0.02	—	—	1	1.8	Petrillo19
HSC J122449–011641	186.20644	-1.27821	19.58	0.59 ± 0.03	—	—	2	1.6	Shu22
HSC J122452+014302	186.21821	1.71746	20.24	0.75 ± 0.03	—	—	2	1.6	Shu22
HSC J122749+003459	186.95500	0.58309	19.09	0.39 ± 0.04	—	—	1,2	1.8	Shu22
HSC J122812+010743	187.05106	1.12887	18.66	0.29 ± 0.05	—	—	1	2.0	C21
HSC J122948+013653	187.45307	1.61498	19.97	0.76 ± 0.02	—	—	1,2	1.6	C21
HSC J123019+004532	187.58074	0.75913	19.71	0.58 ± 0.03	0.580	—	1	2.0	SuGOHI-5
HSC J123636–010215	189.15004	-1.03775	18.47	0.35 ± 0.03	0.418	—	1	1.6	SuGOHI-2
HSC J123648–002834	189.20213	-0.47623	20.68	0.65 ± 0.07	—	—	1	1.8	Shu22
HSC J123803–011006 [‡]	189.51260	-1.16859	18.95	0.33 ± 0.03	—	—	2	1.6	Shu22
HSC J123931–011810 [‡]	189.88330	-1.30285	19.99	0.61 ± 0.03	—	—	1	1.6	Shu22
HSC J124007+013732	190.03235	1.62557	20.11	0.62 ± 0.04	—	—	1,2	1.6	Shu22
HSC J124438–013944	191.16077	-1.66249	18.21	0.36 ± 0.03	0.410	—	1	1.8	SuGOHI-2
HSC J124856–000207	192.23401	-0.03532	19.43	0.51 ± 0.04	0.586	—	1,2	2.2	SuGOHI-2
HSC J125211+002649	193.04897	0.44704	19.62	0.42 ± 0.04	—	—	2	1.8	Shu22
HSC J125251+005805	193.21321	0.96828	19.60	0.56 ± 0.04	0.540	2.435	1,2	2.2	Shu16
HSC J125254+004356	193.22758	0.73229	19.57	0.68 ± 0.03	0.649	—	1,2	2.2	Petrillo19
HSC J125355+001414	193.48197	0.23739	19.97	0.61 ± 0.03	0.638	—	1,2	1.6	SuGOHI-2
HSC J134147+004400	205.44965	0.73346	18.70	0.31 ± 0.04	—	—	1	2.4	Shu22
HSC J134222–014737	205.59517	-1.79369	19.57	0.68 ± 0.03	0.713	—	2	2.2	SuGOHI-2
HSC J134336–010419	205.90035	-1.07199	18.60	0.32 ± 0.03	—	—	1	1.6	Shu22
HSC J134351+010817	205.96651	1.13814	19.46	0.58 ± 0.04	0.567	—	1,2	2.2	SuGOHI-2
HSC J134455–002015	206.23181	-0.33768	18.76	0.38 ± 0.04	—	—	1,2	2.2	SuGOHI-5
HSC J134658–013835	206.74542	-1.64324	18.86	0.42 ± 0.06	—	—	1	1.8	Shu22
HSC J134720–004138	206.83678	-0.69392	21.17	0.73 ± 0.06	—	—	2	1.6	C21
HSC J134816–010646	207.07040	-1.11281	19.80	0.63 ± 0.04	0.620	—	1,2	1.6	Shu22
HSC J134827–003401	207.11666	-0.56699	19.93	0.64 ± 0.04	—	—	2	2.0	C21
HSC J134847+010432	207.19868	1.07563	20.28	0.64 ± 0.05	—	—	2	2.0	C21
HSC J134910–002511 [‡]	207.29500	-0.41995	20.80	0.64 ± 0.05	—	—	1	2.2	Shu22
HSC J135033–004246	207.63874	-0.71298	19.82	0.56 ± 0.04	0.683	—	2	1.8	Shu22
HSC J135038+002550	207.65909	0.43061	19.26	0.54 ± 0.04	0.526	—	1,2	2.2	SuGOHI-2
HSC J135138+002839	207.91213	0.47774	19.39	0.48 ± 0.03	0.461	—	1,2	2.4	SuGOHI-2
HSC J135152+002809	207.96945	0.46919	21.23	0.42 ± 0.05	—	—	1	2.0	Shu22
HSC J135209–010325 [‡]	208.03890	-1.05715	18.24	0.25 ± 0.03	—	—	1	1.6	Shu22
HSC J135242–002613	208.17907	-0.43721	18.68	0.48 ± 0.03	0.508	—	1	2.4	SuGOHI-2
HSC J135252+005530	208.21917	0.92500	21.03	0.74 ± 0.02	—	—	1,2	2.0	SuGOHI-5
HSC J135304+010818	208.26781	1.13840	20.65	0.86 ± 0.04	—	—	2	1.8	Shu22

Continued on next page

Table B.2 – continued from previous page

Name	R.A.	Decl.	m_i	z_d	z_d^{spec}	$z_{\text{source}}^{\text{spec}}$	Classifier	Score	Reference
HSC J135543–005310 [‡]	208.93035	−0.88616	20.86	0.75 ± 0.03	—	—	1,2	2.0	Shu22
HSC J135612–003603	209.05057	−0.60098	21.45	0.80 ± 0.04	—	—	2	1.8	C21
HSC J135620–011030	209.08549	−1.17504	18.68	0.60 ± 0.02	—	—	1,2	1.6	Shu22
HSC J135700–002335	209.25324	−0.39310	20.06	0.70 ± 0.03	—	—	2	1.8	Shu22
HSC J135822+010135	209.59309	1.02661	20.37	0.61 ± 0.05	—	—	2	1.6	Shu22
HSC J135853–021527	209.72294	−2.25762	20.92	0.80 ± 0.09	—	—	1,2	2.4	SuGOHI-2
HSC J135854+013610	209.72600	1.60281	19.12	0.48 ± 0.03	0.504	—	1	2.0	Shu22
HSC J140021+002420	210.08771	0.40573	19.28	0.38 ± 0.04	—	—	1	2.2	SuGOHI-5
HSC J140042–010556	210.17843	−1.09910	20.71	0.74 ± 0.03	—	—	1,2	2.2	SuGOHI-6
HSC J140051–004004	210.21587	−0.66804	19.35	0.34 ± 0.06	—	—	1,2	2.0	C21
HSC J140120–010228	210.33712	−1.04129	19.60	0.42 ± 0.06	—	—	1,2	1.6	C21
HSC J140345–021710	210.93781	−2.28620	19.10	0.55 ± 0.05	0.616	—	1	1.6	SuGOHI-1
HSC J140547–015849	211.44605	−1.98045	20.29	0.65 ± 0.05	—	—	2	2.2	Shu22
HSC J140648+002929	211.70243	0.49158	19.30	0.31 ± 0.05	—	—	1	1.6	SuGOHI-5
HSC J140714–011512	211.80944	−1.25336	20.24	0.60 ± 0.03	—	—	1,2	2.0	C21
HSC J140828+005221	212.11753	0.87258	20.13	0.65 ± 0.04	—	—	2	1.6	Shu22
HSC J140844–005246	212.18452	−0.87969	19.72	0.61 ± 0.04	—	—	1	1.8	SuGOHI-6
HSC J140846–003730	212.19259	−0.62519	19.85	0.59 ± 0.03	—	—	1	1.8	SuGOHI-6
HSC J140854+011017	212.22861	1.17140	18.92	0.37 ± 0.02	—	—	1	1.6	Shu22
HSC J141001+012956	212.50436	1.49916	19.42	0.58 ± 0.04	0.541	—	1,2	2.4	Petrillo19
HSC J141003+011640	212.51300	1.27786	21.00	0.75 ± 0.06	—	—	2	1.6	Shu22
HSC J141129–003129	212.87366	−0.52500	18.41	0.36 ± 0.03	0.360	—	1	2.0	SuGOHI-6
HSC J141137+010720	212.90729	1.12229	19.16	0.47 ± 0.04	0.462	—	1,2	2.2	SuGOHI-5
HSC J141154–012825	212.97770	−1.47362	20.41	0.64 ± 0.05	—	—	1	1.8	Shu22
HSC J141311–011710	213.29602	−1.28636	20.42	0.59 ± 0.05	—	—	1	1.6	Shu22
HSC J141311+003724	213.29827	0.62341	19.86	0.62 ± 0.03	0.698	—	1	2.0	Shu22
HSC J141435+010928	213.64967	1.15794	19.81	0.62 ± 0.03	—	—	2	2.0	Shu22
HSC J141446–005837	213.69563	−0.97699	20.33	0.62 ± 0.05	—	—	2	1.6	Shu22
HSC J141516–000332 [‡]	213.81944	−0.05889	20.41	0.55 ± 0.04	—	—	1	2.2	Shu22
HSC J141619+434224	214.07985	43.70689	19.82	0.47 ± 0.03	—	—	1	1.8	C21
HSC J141635+010128	214.14762	1.02468	20.28	0.70 ± 0.04	0.700	—	1,2	2.4	SuGOHI-1
HSC J141647+432035 [‡]	214.19919	43.34314	20.18	0.67 ± 0.05	—	—	1,2	1.6	Shu22
HSC J141649+013822	214.20756	1.63951	18.31	0.31 ± 0.03	—	—	1,2	2.4	Petrillo19
HSC J141728+015935	214.36704	1.99310	18.36	0.34 ± 0.03	0.401	—	1,2	2.0	Petrillo19
HSC J141805+003958 [‡]	214.52252	0.66638	19.78	0.58 ± 0.04	—	—	2	1.6	Shu22
HSC J141807+003925	214.52998	0.65710	19.25	0.52 ± 0.03	0.531	—	1,2	1.6	SuGOHI-6
HSC J141831–000052	214.63086	−0.01464	18.00	0.25 ± 0.02	0.263	—	1	2.2	SuGOHI-1
HSC J141846+010837	214.69279	1.14378	20.20	0.58 ± 0.05	—	—	2	1.8	Shu22
HSC J141905–010739	214.77452	−1.12759	20.97	0.78 ± 0.03	—	—	2	2.0	SuGOHI-6
HSC J141930+434129	214.87668	43.69162	19.91	0.56 ± 0.04	0.545	—	1	1.6	Shu22
HSC J142009–001434	215.03773	−0.24288	19.61	0.60 ± 0.03	0.615	—	1,2	2.0	SuGOHI-1
HSC J142037+020231 [‡]	215.15771	2.04199	18.50	0.37 ± 0.02	0.392	—	1	1.8	Shu22
HSC J142048+000733	215.20170	0.12607	21.00	0.60 ± 0.05	—	—	2	1.8	SuGOHI-5
HSC J142049+013235	215.20680	1.54319	20.13	0.54 ± 0.04	—	—	2	1.8	Shu22
HSC J142102+011319 [‡]	215.26121	1.22213	20.01	0.55 ± 0.05	—	—	1,2	1.8	Shu22
HSC J142103+002219	215.26538	0.37196	20.38	0.67 ± 0.04	—	—	1,2	2.4	Huang20
HSC J142232+000134	215.63464	0.02625	17.51	0.25 ± 0.02	0.277	—	1	2.0	Petrillo19
HSC J142241+424608	215.67170	42.76890	20.19	0.63 ± 0.06	0.605	—	1,2	1.8	SuGOHI-2
HSC J142301–002748 [‡]	215.75532	−0.46357	21.02	0.73 ± 0.06	—	—	1,2	1.8	Shu22
HSC J142318–001227	215.82580	−0.20771	21.00	0.72 ± 0.05	—	—	1,2	2.4	C21
HSC J142353+013446	215.97109	1.57970	19.33	0.51 ± 0.03	0.519	—	1,2	2.0	SuGOHI-2
HSC J142410–005317	216.04510	−0.88810	20.72	0.88 ± 0.04	—	—	1,2	2.0	SuGOHI-6
HSC J142459+005506	216.24984	0.91850	19.73	0.55 ± 0.04	0.551	—	2	2.0	C21
HSC J142502+013057	216.26121	1.51601	19.61	0.56 ± 0.04	—	—	2	1.8	SuGOHI-6
HSC J142518–002525	216.32777	−0.42373	19.85	0.61 ± 0.03	—	—	1	2.0	SuGOHI-6
HSC J142528–011504	216.36694	−1.25125	19.44	0.54 ± 0.04	0.568	—	2	1.6	SuGOHI-6
HSC J142619+010535	216.58236	1.09333	18.19	0.29 ± 0.03	0.324	—	1	1.6	Shu22
HSC J142652+433113 [‡]	216.71748	43.52044	18.76	0.54 ± 0.03	0.577	—	1	1.6	Shu22
HSC J142720+001916	216.83560	0.32111	19.35	0.56 ± 0.03	0.551	1.266	1	2.4	SuGOHI-1
HSC J142754+003944	216.97863	0.66239	20.86	0.85 ± 0.04	—	—	1	2.4	SuGOHI-6

Continued on next page

Table B.2 – continued from previous page

Name	R.A.	Decl.	m_i	z_d	z_d^{spec}	$z_{\text{source}}^{\text{spec}}$	Classifier	Score	Reference
HSC J142811–005021	217.04855	−0.83923	19.43	0.65 ± 0.03	—	—	1,2	1.8	SuGOHI-6
HSC J142823–014829	217.09736	−1.80832	18.37	0.28 ± 0.03	0.280	—	1	1.8	Shu22
HSC J143113–000613	217.80786	−0.10374	20.58	0.72 ± 0.04	—	—	1,2	2.2	SuGOHI-5
HSC J143135–015445	217.89596	−1.91277	19.16	0.51 ± 0.04	0.520	—	1	1.8	Shu22
HSC J143150+013019	217.96190	1.50549	19.84	0.75 ± 0.03	0.754	—	1,2	2.2	SuGOHI-6
HSC J143153–013352	217.97250	−1.56450	20.51	0.69 ± 0.04	0.671	—	1,2	2.4	SuGOHI-6
HSC J143210–004234 [‡]	218.04516	−0.70958	19.12	0.39 ± 0.05	—	—	1	1.6	Shu22
HSC J143243–004553	218.18311	−0.76486	19.23	0.46 ± 0.03	0.466	—	1	2.2	SuGOHI-6
HSC J143419+433525	218.57928	43.59039	19.19	0.62 ± 0.03	0.690	—	1	1.8	Shu22
HSC J143444–000948	218.68635	−0.16350	18.98	0.55 ± 0.03	0.550	—	1,2	2.2	SuGOHI-6
HSC J143714–015323 [‡]	219.31209	−1.88972	20.27	0.66 ± 0.05	—	—	1	2.0	Shu22
HSC J143746+432259	219.44438	43.38330	19.62	0.59 ± 0.07	0.563	—	1	1.8	C21
HSC J143832–002326	219.63533	−0.39081	20.70	0.88 ± 0.03	—	—	2	1.8	SuGOHI-5
HSC J143837+005739	219.65428	0.96084	18.61	0.29 ± 0.03	—	—	1	2.0	Shu22
HSC J143901+005117	219.75576	0.85495	20.24	0.78 ± 0.03	—	—	1,2	2.4	SuGOHI-6
HSC J143932+005358	219.88697	0.89945	17.09	0.23 ± 0.02	0.313	—	1	2.4	Petrillo19
HSC J143955–002733	219.98188	−0.45923	19.99	0.53 ± 0.04	0.542	—	1,2	1.6	SuGOHI-5
HSC J144226–005804	220.61041	−0.96788	19.59	0.38 ± 0.06	—	—	2	1.8	Shu22
HSC J144228+002105	220.61990	0.35151	18.09	0.19 ± 0.14	—	—	1	2.0	Shu22
HSC J144230–002353	220.62905	−0.39812	18.54	0.40 ± 0.05	0.370	—	1	2.2	Petrillo19
HSC J144242+422315	220.67508	42.38777	19.24	0.52 ± 0.03	0.542	—	1	1.8	C21
HSC J144301+011159	220.75454	1.19989	19.73	0.76 ± 0.03	—	—	1,2	1.8	SuGOHI-6
HSC J144302+441723	220.76151	44.28983	18.38	0.33 ± 0.03	0.317	—	1	2.0	Guoyou Sun
HSC J144307–004056	220.77985	−0.68227	18.94	0.59 ± 0.03	0.500	1.071	1,2	2.2	SuGOHI-1
HSC J144428–005142	221.11975	−0.86181	19.68	0.60 ± 0.04	0.575	—	1,2	2.2	Petrillo19
HSC J144640–000350	221.66715	−0.06397	21.18	0.97 ± 0.06	—	—	1,2	2.2	SuGOHI-6
HSC J144643–004534	221.68014	−0.75952	20.09	0.71 ± 0.04	—	—	2	1.8	SuGOHI-6
HSC J145037–004543	222.65725	−0.76214	20.17	0.76 ± 0.02	—	—	1	2.2	SuGOHI-6
HSC J145058–005521	222.74463	−0.92258	17.99	0.29 ± 0.03	0.323	—	1	1.8	Shu22
HSC J145103–000526	222.76457	−0.09071	19.73	0.52 ± 0.03	0.505	—	1	1.6	SuGOHI-1
HSC J145106+011133	222.77664	1.19266	18.05	0.33 ± 0.03	0.391	—	1	1.6	Petrillo19
HSC J145123+440738	222.84963	44.12749	19.00	0.33 ± 0.03	—	—	1,2	1.8	C21
HSC J145129+425535	222.87356	42.92653	19.88	0.66 ± 0.10	—	—	1,2	1.8	Shu22
HSC J145218+434318	223.07694	43.72188	20.54	0.62 ± 0.05	—	—	1,2	1.6	C21
HSC J145230+001626	223.12881	0.27391	20.84	0.66 ± 0.05	—	—	1	2.0	C21
HSC J145242+425731	223.17884	42.95884	19.91	0.73 ± 0.02	0.718	—	1,2	2.4	SuGOHI-2
HSC J145320–001826	223.33385	−0.30723	20.09	0.74 ± 0.03	—	—	2	1.6	SuGOHI-5
HSC J145325–003332	223.35741	−0.55890	19.28	0.43 ± 0.05	—	—	1,2	1.8	SuGOHI-6
HSC J145402+013809	223.51216	1.63601	19.41	0.53 ± 0.03	0.537	—	1	2.0	SuGOHI-2
HSC J145615+432531	224.06523	43.42549	19.31	0.53 ± 0.03	—	—	1,2	1.6	Shu22
HSC J145631–000848	224.13243	−0.14676	20.29	0.62 ± 0.04	—	—	2	1.6	Shu22
HSC J145640+425642	224.16992	42.94525	17.66	0.28 ± 0.02	0.284	—	1	2.2	Shu22
HSC J145659+435249	224.24939	43.88051	18.43	0.51 ± 0.03	0.560	—	1	1.8	Shu22
HSC J145734+434044 [‡]	224.39265	43.67893	19.71	0.47 ± 0.03	0.490	—	2	2.0	Shu22
HSC J145759+423019	224.49667	42.50528	19.52	0.60 ± 0.05	0.607	—	1	2.0	SuGOHI-2
HSC J145902–012351	224.76135	−1.39757	19.54	0.48 ± 0.03	0.482	—	1	2.4	SuGOHI-1
HSC J145922+011912	224.84180	1.32022	19.93	0.70 ± 0.04	0.703	—	1	1.6	SuGOHI-1
HSC J145932–000120	224.88666	−0.02235	18.17	0.35 ± 0.05	0.439	—	1	1.6	Shu22
HSC J150015+001908	225.06437	0.31890	21.48	0.85 ± 0.03	—	—	1,2	1.6	C21
HSC J150023+012833 [‡]	225.09595	1.47586	20.57	0.70 ± 0.06	—	—	2	2.0	Shu22
HSC J150029+015119	225.12292	1.85548	19.77	0.52 ± 0.03	0.529	—	1,2	1.8	SuGOHI-2
HSC J150053+002202	225.22323	0.36735	21.17	0.74 ± 0.04	—	—	2	1.6	Shu22
HSC J150239–001914	225.66454	−0.32056	17.60	0.30 ± 0.03	0.329	—	1	1.8	SuGOHI-6
HSC J150438+424601	226.16012	42.76699	20.27	0.62 ± 0.04	—	—	2	1.6	C21
HSC J150712+420944	226.80114	42.16226	18.77	0.47 ± 0.08	0.486	—	1	2.0	SuGOHI-2
HSC J151123+433333	227.84767	43.55922	21.42	0.84 ± 0.04	—	—	2	1.8	C21
HSC J151336+433250	228.40322	43.54750	18.93	0.46 ± 0.05	0.487	—	1,2	2.2	SuGOHI-2
HSC J151710+440740 [‡]	229.29540	44.12779	20.83	0.63 ± 0.09	—	—	2	2.0	Shu22
HSC J151814+441613	229.56017	44.27042	19.05	0.63 ± 0.03	—	—	1	1.8	Shu22
HSC J152217+425738	230.57121	42.96079	19.01	0.33 ± 0.04	—	—	1	1.6	SuGOHI-5

Continued on next page

Table B.2 – continued from previous page

Name	R.A.	Decl.	m_i	z_d	z_d^{spec}	$z_{\text{source}}^{\text{spec}}$	Classifier	Score	Reference
HSC J152632+440616	231.63630	44.10446	19.89	0.49 ± 0.03	0.487	—	1,2	1.8	SuGOHI-5
HSC J153342+425022	233.42898	42.83966	19.52	0.61 ± 0.04	—	—	1,2	2.0	C21
HSC J153738+423425	234.41083	42.57385	20.19	0.62 ± 0.04	—	—	1	1.8	Shu22
HSC J153825+435718	234.60656	43.95513	20.17	0.67 ± 0.06	—	—	1	1.6	C21
HSC J154547+432648	236.44590	43.44686	18.64	0.48 ± 0.03	0.503	—	1	2.0	SuGOHI-6
HSC J154722+420735	236.84572	42.12664	20.08	0.73 ± 0.03	0.753	—	1	2.0	Shu22
HSC J154912+434556	237.30005	43.76569	17.90	0.28 ± 0.04	0.234	—	1	1.6	Shu22
HSC J155112+430009	237.80048	43.00257	20.07	0.53 ± 0.05	—	—	1,2	2.0	Shu22
HSC J155358+425933	238.49572	42.99266	20.27	0.64 ± 0.05	—	—	1,2	2.0	SuGOHI-6
HSC J155619+422855	239.08122	42.48198	20.00	0.74 ± 0.05	—	—	2	2.0	SuGOHI-6
HSC J155625+432413	239.10825	43.40368	21.04	0.88 ± 0.06	—	—	2	2.0	Shu22
HSC J160052+441303	240.22003	44.21755	19.54	0.55 ± 0.03	0.547	—	1	2.0	SuGOHI-1
HSC J160307+431421	240.78050	43.23936	19.06	0.55 ± 0.03	0.543	—	1	2.2	SuGOHI-6
HSC J160611+441930	241.54992	44.32505	20.20	0.71 ± 0.03	—	—	1	1.6	SuGOHI-6
HSC J160815+420009	242.06516	42.00263	20.66	0.68 ± 0.05	0.615	—	2	2.0	SuGOHI-5
HSC J161209+425752	243.03921	42.96461	18.36	0.38 ± 0.04	—	—	1	2.0	SuGOHI-6
HSC J161221+424908	243.09028	42.81916	21.60	0.79 ± 0.02	—	—	2	1.6	C21
HSC J161538+422637	243.90958	42.44381	19.97	0.68 ± 0.04	0.656	—	1,2	1.6	SuGOHI-1
HSC J161633+431457	244.14133	43.24929	20.24	0.74 ± 0.06	—	—	2	2.0	C21
HSC J162029+434216	245.12193	43.70446	19.98	0.75 ± 0.02	0.687	—	1	1.8	SuGOHI-6
HSC J162452+424221	246.21935	42.70590	17.97	0.31 ± 0.03	0.351	—	1	2.0	Shu22
HSC J163050+440154	247.70969	44.03189	19.66	0.55 ± 0.04	0.532	—	1,2	1.6	SuGOHI-1
HSC J163108+423442	247.78636	42.57839	20.38	0.72 ± 0.08	—	—	1	1.6	SuGOHI-5
HSC J163417+434634	248.57084	43.77636	20.92	0.69 ± 0.05	—	—	1,2	2.2	Shu22
HSC J163907+424611	249.77981	42.76980	19.11	0.47 ± 0.03	0.518	—	1	1.6	SuGOHI-5
HSC J164033+423028	250.13794	42.50781	21.58	0.86 ± 0.06	—	—	2	1.6	Shu22
HSC J220335+045535	330.89983	4.92654	18.60	0.37 ± 0.04	0.411	—	1	2.0	Shu22
HSC J220506+014703	331.27881	1.78434	19.65	0.49 ± 0.03	0.476	2.526	1	2.2	More12
HSC J220550+041524	331.45907	4.25687	17.66	0.23 ± 0.02	0.268	—	1	2.0	SuGOHI-2
HSC J220724+013833	331.85042	1.64266	20.42	0.70 ± 0.06	—	—	1	1.6	C21
HSC J221101+003401	332.75826	0.56703	20.06	0.68 ± 0.05	0.676	—	1,2	2.4	SuGOHI-1
HSC J221206–001359	333.02646	-0.23311	19.74	0.31 ± 0.08	—	—	2	1.6	Shu22
HSC J221222–001811	333.09502	-0.30318	21.53	0.98 ± 0.02	—	—	2	1.8	Jacobs17
HSC J221234+045456	333.14375	4.91582	18.51	0.26 ± 0.03	0.262	—	1	2.2	SuGOHI-2
HSC J221306–003036	333.27886	-0.51025	19.82	0.69 ± 0.05	0.703	—	1,2	2.0	More12
HSC J221315+034536	333.31367	3.76022	18.96	0.40 ± 0.04	0.446	—	1,2	1.6	SuGOHI-2
HSC J221320+035434	333.33406	3.90945	20.90	0.67 ± 0.06	—	—	1	2.0	SuGOHI-5
HSC J221412+040335 [‡]	333.55202	4.05993	19.31	0.49 ± 0.03	0.512	—	1	1.8	Shu22
HSC J221455+012932	333.73159	1.49231	19.78	0.62 ± 0.04	0.591	—	1	1.8	Shu22
HSC J221513+010240	333.80563	1.04458	20.42	0.73 ± 0.03	—	—	1,2	1.8	Diehl17
HSC J221522+010528	333.84287	1.09117	20.68	0.50 ± 0.05	—	—	2	1.8	SuGOHI-5
HSC J221726+000350	334.36018	0.06395	18.60	0.37 ± 0.03	0.398	—	1	2.0	SuGOHI-1
HSC J221852+014038	334.71929	1.67748	19.39	0.55 ± 0.03	0.564	—	1,2	1.8	Sonnenfeld13
HSC J221936+014416	334.90038	1.73804	19.60	0.56 ± 0.03	0.678	—	1	1.8	SuGOHI-1
HSC J222002+060506	335.00848	6.08526	18.89	0.40 ± 0.05	0.308	—	1	1.6	C21
HSC J222041+004912	335.17256	0.82009	20.04	0.82 ± 0.02	0.838	—	1	2.0	SuGOHI-6
HSC J222116–002829	335.31960	-0.47500	20.19	0.61 ± 0.04	0.609	—	2	2.0	SuGOHI-6
HSC J222140+025339	335.41827	2.89437	20.27	0.61 ± 0.05	—	—	2	2.0	Shu22
HSC J222142+025655	335.42662	2.94873	20.11	0.84 ± 0.02	—	—	1	1.8	SuGOHI-6
HSC J222201+044004	335.50556	4.66794	20.60	0.70 ± 0.06	—	—	1	1.8	Shu22
HSC J222217+001202	335.57353	0.20079	19.38	0.41 ± 0.08	0.436	1.360	1	2.0	Sonnenfeld13
HSC J222301–000527	335.75573	-0.09088	17.80	0.28 ± 0.03	0.317	—	1	1.6	SuGOHI-6
HSC J222356+042809	335.98621	4.46942	19.21	0.41 ± 0.03	—	—	1,2	1.8	C21
HSC J222503–004007	336.26280	-0.66874	21.50	0.83 ± 0.03	—	—	2	1.8	SuGOHI-6
HSC J222638–003449	336.65957	-0.58042	18.84	0.41 ± 0.06	0.404	—	1,2	2.4	SuGOHI-5
HSC J222651–002206	336.71551	-0.36845	19.38	0.47 ± 0.03	0.469	—	1	1.6	Shu22
HSC J222653+035502	336.72154	3.91726	20.01	0.66 ± 0.04	0.698	—	2	2.0	C21
HSC J222801+012805	337.00825	1.46822	19.82	0.64 ± 0.05	0.647	2.462	1,2	2.0	SuGOHI-1
HSC J222834+004009 [‡]	337.14221	0.66939	20.61	0.65 ± 0.05	0.632	—	1	1.8	Shu22
HSC J223032–003922	337.63418	-0.65617	18.64	0.38 ± 0.03	0.402	—	1	1.8	SuGOHI-6
HSC J223207+025548	338.03145	2.93006	19.82	0.59 ± 0.03	0.688	—	1	2.0	Shu22

Continued on next page

Table B.2 – continued from previous page

Name	R.A.	Decl.	m_i	z_d	z_d^{spec}	$z_{\text{source}}^{\text{spec}}$	Classifier	Score	Reference
HSC J223211+015955	338.04845	1.99869	20.06	0.66 ± 0.05	0.634	—	1	2.0	SuGOHI-6
HSC J223212+031330	338.05069	3.22517	20.23	0.73 ± 0.03	0.704	—	1,2	2.2	C21
HSC J223227+041457	338.11445	4.24938	21.12	0.85 ± 0.03	—	—	1,2	1.6	Shu22
HSC J223238–002533	338.16103	-0.42604	21.25	1.02 ± 0.05	—	—	2	2.0	SuGOHI-5
HSC J223324+012521	338.35268	1.42258	20.98	0.83 ± 0.04	0.861	—	2	1.8	SuGOHI-6
HSC J223406+012057	338.52904	1.34924	19.90	0.78 ± 0.02	0.670	—	1,2	1.6	SuGOHI-1
HSC J223443+030307	338.68304	3.05218	19.92	0.59 ± 0.03	—	—	1,2	2.2	SuGOHI-6
HSC J223513+034313	338.80625	3.72041	20.59	0.61 ± 0.04	0.632	—	1,2	2.2	C21
HSC J223555+011031	338.98132	1.17535	20.71	0.72 ± 0.04	—	—	2	1.6	C21
HSC J223607–003605	339.03303	-0.60154	20.40	0.64 ± 0.05	0.583	—	2	1.8	Shu22
HSC J223650+022221	339.20941	2.37253	20.98	0.67 ± 0.05	—	—	2	2.4	Shu22
HSC J223654–010745	339.22575	-1.12935	20.43	0.74 ± 0.11	0.625	—	1	2.0	Shu22
HSC J223720–004008	339.33574	-0.66916	20.87	0.60 ± 0.04	—	—	2	2.0	Shu22
HSC J223735+004014	339.39736	0.67075	18.25	0.32 ± 0.05	—	—	1	2.0	SuGOHI-6
HSC J223744+005339	339.43453	0.89429	20.08	0.62 ± 0.04	0.621	—	1,2	1.6	SuGOHI-1
HSC J223931+000525	339.87924	0.09036	19.65	0.66 ± 0.05	0.658	—	1	1.8	SuGOHI-6
HSC J223947+040001 [‡]	339.94929	4.00049	22.13	0.96 ± 0.08	—	—	2	1.6	Shu22
HSC J224021+030150	340.09124	3.03080	19.55	0.42 ± 0.04	—	—	1	1.8	Shu22
HSC J224101+041820 ^{†‡}	340.25666	4.30566	19.63	0.68 ± 0.03	0.592	—	1	1.8	Shu22
HSC J224116+042934	340.31963	4.49295	20.50	0.70 ± 0.06	—	—	1	1.6	Shu22
HSC J224150+043038	340.46164	4.51062	20.32	0.55 ± 0.04	0.597	—	1	1.8	Shu22
HSC J224154+000331	340.47761	0.05875	19.68	0.59 ± 0.04	—	—	2	2.4	SuGOHI-6
HSC J224411+013819	341.04904	1.63883	19.49	0.52 ± 0.03	0.535	—	1	1.8	SuGOHI-6
HSC J224614+055828	341.56090	5.97459	18.51	0.27 ± 0.03	0.340	—	1	2.2	SuGOHI-5
HSC J224800–010259	342.00300	-1.04990	17.25	0.23 ± 0.02	0.277	—	1	1.8	SuGOHI-2
HSC J224804+023036	342.01727	2.51009	18.69	0.39 ± 0.04	0.428	—	1	1.8	SuGOHI-6
HSC J224836–012334	342.15147	-1.39282	19.03	0.41 ± 0.04	0.398	—	1	2.2	Jacobs19b
HSC J224942–002625	342.42878	-0.44046	19.24	0.48 ± 0.03	0.498	—	1	2.0	Shu22
HSC J225012+053939	342.55098	5.66104	20.66	0.73 ± 0.04	—	—	1	1.6	Shu22
HSC J225019+004803	342.57943	0.80110	19.49	0.49 ± 0.04	0.530	—	1	1.8	SuGOHI-1
HSC J225052+052053	342.71673	5.34816	21.06	0.77 ± 0.03	0.764	—	2	1.6	Shu22
HSC J225122+052527	342.84504	5.42426	19.31	0.35 ± 0.05	—	—	1	2.4	C21
HSC J225153+051518 [‡]	342.97144	5.25520	20.52	0.76 ± 0.01	—	—	2	2.2	Shu22
HSC J225209+011741	343.03813	1.29490	20.64	0.79 ± 0.04	—	—	1	1.8	Shu22
HSC J225241+041658 [‡]	343.17400	4.28300	20.10	0.61 ± 0.04	—	—	2	1.6	Shu22
HSC J225317+040045	343.32126	4.01261	19.71	0.64 ± 0.05	0.642	—	1,2	2.0	Shu22
HSC J225324+015005	343.35009	1.83486	19.12	0.46 ± 0.03	0.471	—	1	1.8	SuGOHI-5
HSC J225615+034052	344.06440	3.68123	19.67	0.68 ± 0.03	—	—	1	2.0	C21
HSC J225921+023331	344.83865	2.55889	20.12	0.65 ± 0.04	0.628	—	2	2.2	C21
HSC J230335+003703	345.89653	0.61754	18.88	0.44 ± 0.05	0.458	0.936	1	2.2	Brownstein12
HSC J230545+000540	346.44017	0.09455	20.54	0.73 ± 0.05	—	—	1,2	2.4	C21
HSC J230658+022543	346.74281	2.42866	18.13	0.33 ± 0.03	0.362	—	1	2.2	SuGOHI-2
HSC J230954+013712	347.47829	1.62004	20.17	0.68 ± 0.04	0.625	—	1,2	2.2	C21
HSC J231001+013550	347.50731	1.59741	19.81	0.59 ± 0.04	0.573	—	1,2	1.8	SuGOHI-2
HSC J231021+015451	347.58759	1.91441	20.29	0.62 ± 0.10	—	—	1,2	2.2	C21
HSC J231145–013039	347.93784	-1.51084	18.31	0.34 ± 0.03	0.400	—	1	2.2	SuGOHI-2
HSC J231253–001112	348.22399	-0.18686	19.58	0.58 ± 0.03	0.586	—	1	1.6	SuGOHI-2
HSC J231334+003411 [‡]	348.39242	0.56972	19.40	0.39 ± 0.04	—	—	1	1.8	Shu22
HSC J231416–000310	348.56728	-0.05296	19.12	0.58 ± 0.03	—	—	1	2.2	SuGOHI-5
HSC J231416+000609	348.57080	0.10276	19.55	0.47 ± 0.04	—	—	1	2.0	C21
HSC J231431+013548	348.63053	1.59682	19.57	0.55 ± 0.03	0.524	—	1,2	2.2	SuGOHI-5
HSC J231451+020635	348.71581	2.10990	20.02	0.59 ± 0.03	—	—	1	1.8	Shu22
HSC J231539–005248	348.91596	-0.88023	19.53	0.47 ± 0.03	0.473	—	2	2.4	C21
HSC J231621+014836	349.09118	1.81014	19.66	0.58 ± 0.03	0.579	—	1	2.2	SuGOHI-5
HSC J231647+013715	349.19653	1.62100	20.32	0.57 ± 0.04	—	—	1,2	2.2	C21
HSC J231926–001124 [‡]	349.85903	-0.19012	19.74	0.56 ± 0.03	0.555	—	1	2.2	Shu22
HSC J232036–005510	350.15215	-0.91949	18.98	0.45 ± 0.03	0.469	—	1	2.2	Shu22
HSC J232042+015439	350.17780	1.91091	20.07	0.47 ± 0.03	—	—	2	1.8	Shu22
HSC J232142+013753	350.42732	1.63165	19.86	0.53 ± 0.03	0.558	—	1,2	1.6	Shu22
HSC J232143–000214 [‡]	350.43021	-0.03742	20.06	0.61 ± 0.04	—	—	2	2.0	Shu22

Continued on next page

Table B.2 – continued from previous page

Name	R.A.	Decl.	m_i	z_d	z_d^{spec}	$z_{\text{source}}^{\text{spec}}$	Classifier	Score	Reference
HSC J232148–011948	350.45029	−1.33025	19.09	0.54 ± 0.02	0.593	—	2	1.8	Shu22
HSC J232159–003754	350.49868	−0.63187	18.56	0.36 ± 0.05	—	—	1,2	1.6	C21
HSC J232225–001529	350.60699	−0.25817	20.37	0.77 ± 0.03	0.754	—	1	2.0	Shu22
HSC J232249+003915	350.70649	0.65435	19.35	0.61 ± 0.04	0.710	—	1	1.6	Shu22
HSC J232415+011331	351.06513	1.22552	19.75	0.69 ± 0.01	0.593	—	1,2	2.2	SuGOHI-2
HSC J232451+002700	351.21623	0.45010	19.81	0.73 ± 0.03	—	—	1	2.4	Shu22
HSC J232509+005111	351.28928	0.85322	20.02	0.51 ± 0.04	0.504	—	2	2.4	C21
HSC J232547+003739	351.44998	0.62764	18.95	0.44 ± 0.04	0.468	—	1,2	2.4	C21
HSC J232839–004640	352.16351	−0.77779	18.76	0.35 ± 0.03	0.350	—	1	1.6	Shu22
HSC J232934–001137	352.39402	−0.19366	21.16	0.78 ± 0.08	—	—	2	2.0	Shu22
HSC J233047–000231	352.69800	−0.04203	17.99	0.27 ± 0.03	0.298	—	1	2.0	SuGOHI-5
HSC J233311+022311	353.29631	2.38641	20.38	0.50 ± 0.04	0.472	2.253	2	1.8	Shu16
HSC J233608+005406	354.03482	0.90167	20.82	0.65 ± 0.05	—	—	2	1.6	Stein21
HSC J233633+003838	354.13826	0.64390	19.28	0.32 ± 0.04	—	—	2	1.8	Shu22
HSC J233945+015726	354.93788	1.95747	19.79	0.50 ± 0.03	0.505	—	1	1.6	Guoyou Sun
HSC J234117–002937	355.32304	−0.49388	19.12	0.51 ± 0.04	0.531	—	1,2	2.2	C21
HSC J234124–003058	355.35285	−0.51625	19.51	0.48 ± 0.09	—	—	1,2	2.2	C21
HSC J234248–012032	355.70284	−1.34239	19.55	0.58 ± 0.04	0.527	2.265	1	1.8	Shu16
HSC J234251–001502	355.71363	−0.25058	18.26	0.29 ± 0.04	0.387	—	1	1.8	SuGOHI-5
HSC J234345+014702 [‡]	355.94027	1.78413	20.15	0.60 ± 0.04	—	—	1	1.6	Shu22
HSC J234421+001211	356.08955	0.20331	20.10	0.75 ± 0.02	0.655	—	1,2	1.8	Shu22
HSC J234637+004609	356.65608	0.76918	18.69	0.60 ± 0.03	0.605	—	1	2.2	C21
HSC J234723+003219 [‡]	356.84999	0.53874	19.35	0.64 ± 0.04	0.623	—	1	1.6	Shu22
HSC J234845+014834	357.18919	1.80959	19.82	0.62 ± 0.03	0.590	—	1	1.6	Shu22
HSC J235042+024809 [‡]	357.67833	2.80277	19.82	0.60 ± 0.03	—	—	1	1.8	Shu22
HSC J235211+000615	358.04899	0.10441	21.59	0.75 ± 0.12	—	—	1,2	1.8	SuGOHI-5
HSC J235328+004041	358.37029	0.67821	20.48	0.66 ± 0.05	—	—	1	1.6	Shu22
HSC J235353+021246	358.47152	2.21297	18.71	0.49 ± 0.03	0.493	—	1	2.0	Shu22
HSC J235730+010133	359.37764	1.02596	19.75	0.64 ± 0.04	0.638	—	1,2	2.2	C21
HSC J235813–000036	359.55563	−0.01010	19.97	0.60 ± 0.03	0.627	—	1	1.6	Shu22
HSC J235821+021156	359.58788	2.19909	18.88	0.39 ± 0.04	0.423	—	1	1.8	Shu22
HSC J235853+012406	359.72171	1.40182	19.92	0.55 ± 0.08	0.481	—	1,2	2.2	Huang21

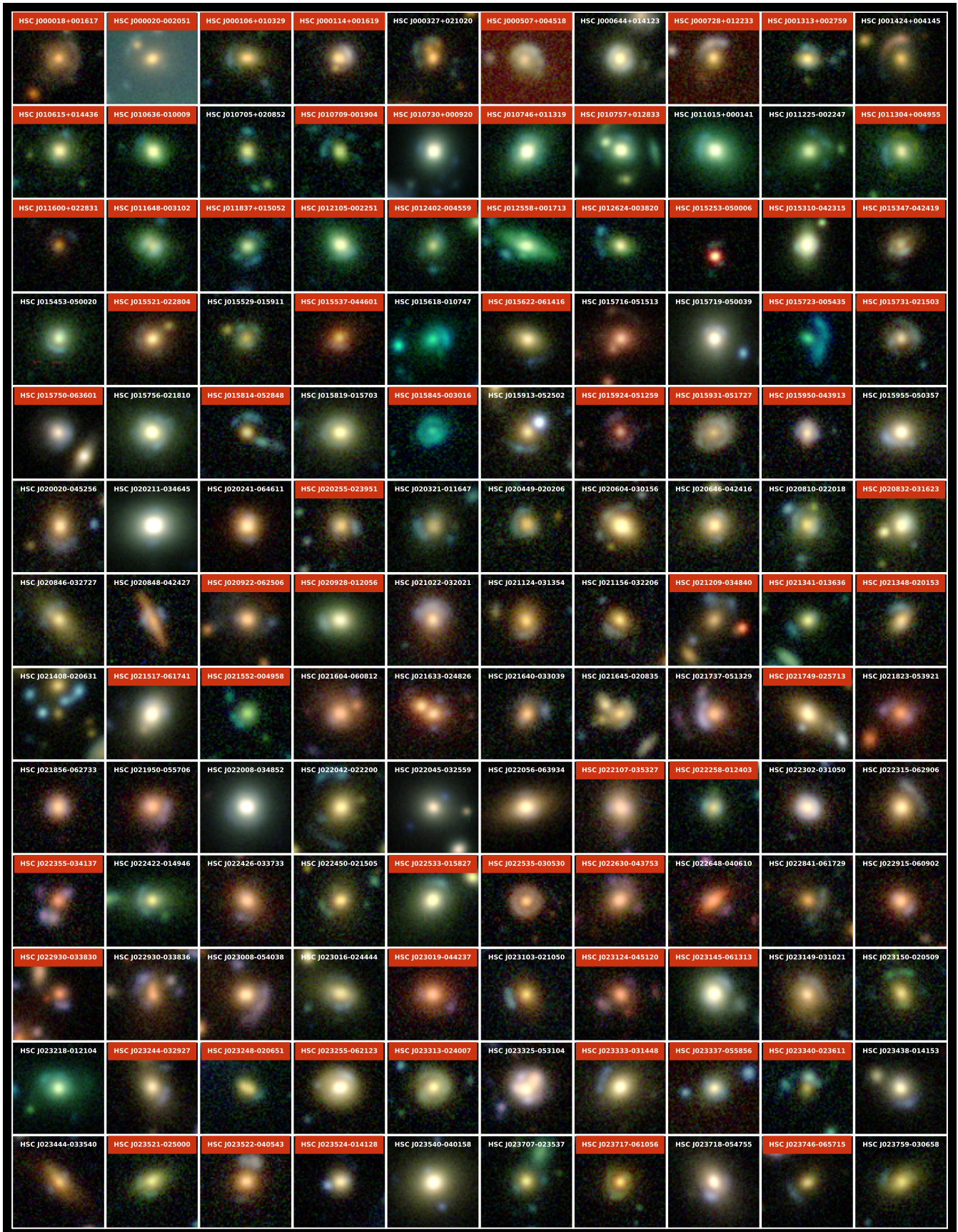


Fig. B.1: Colour composite images ($10'' \times 10''$) of the 630 grade-B strong-lens candidates discovered by this work. Candidates with red background beneath the system name are new discoveries.

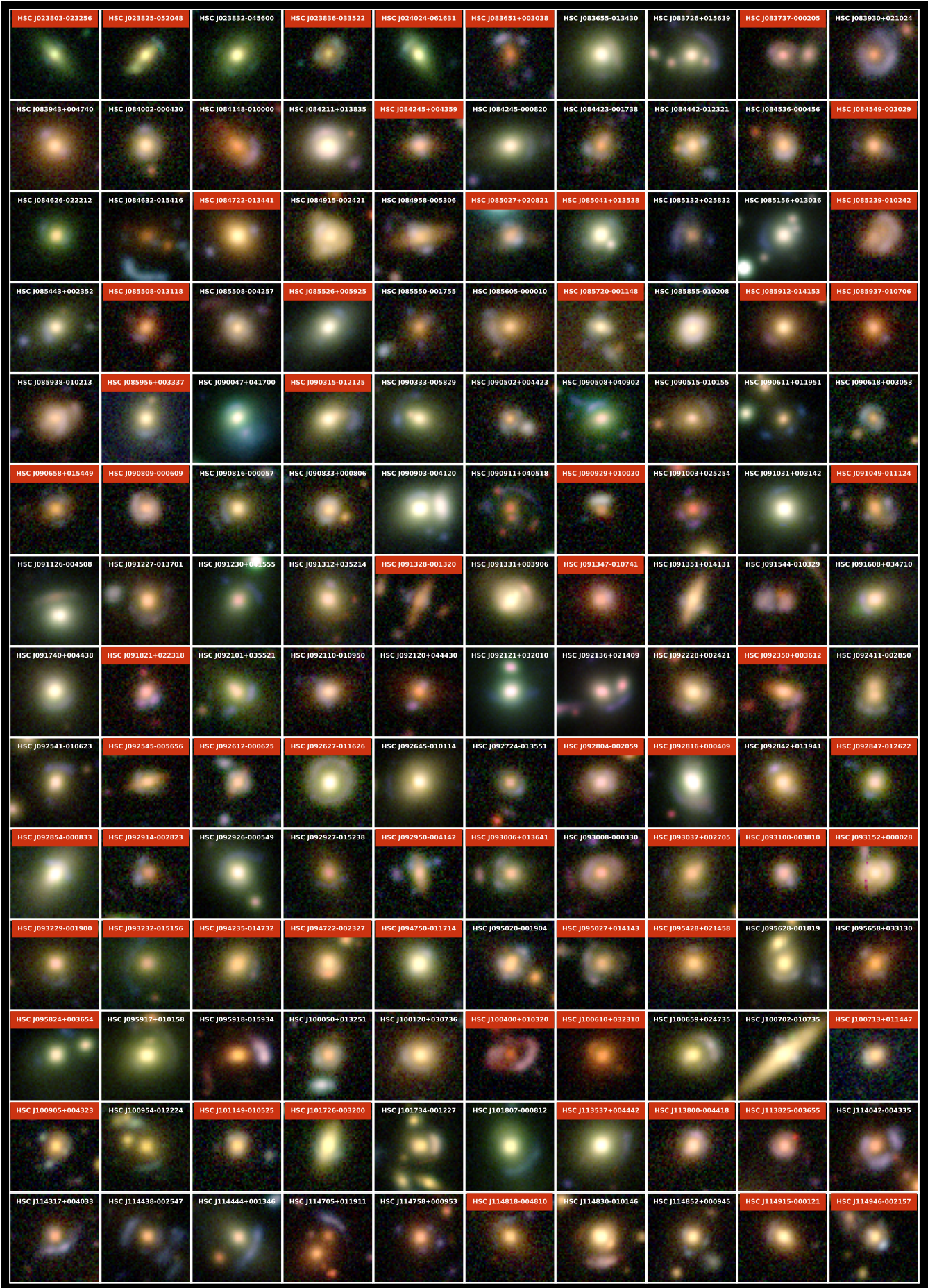


Fig. B.1: continued

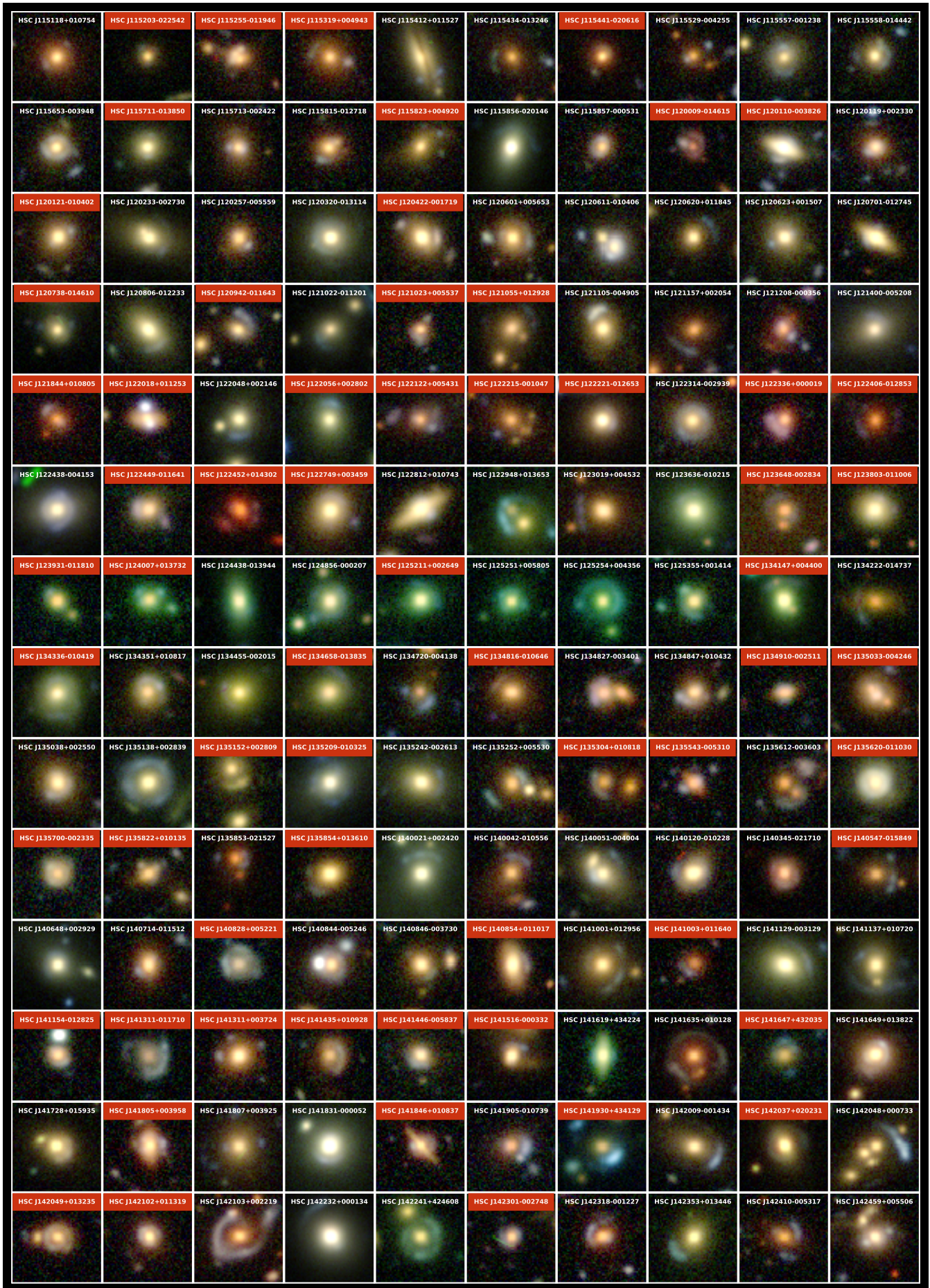


Fig. B.1: continued

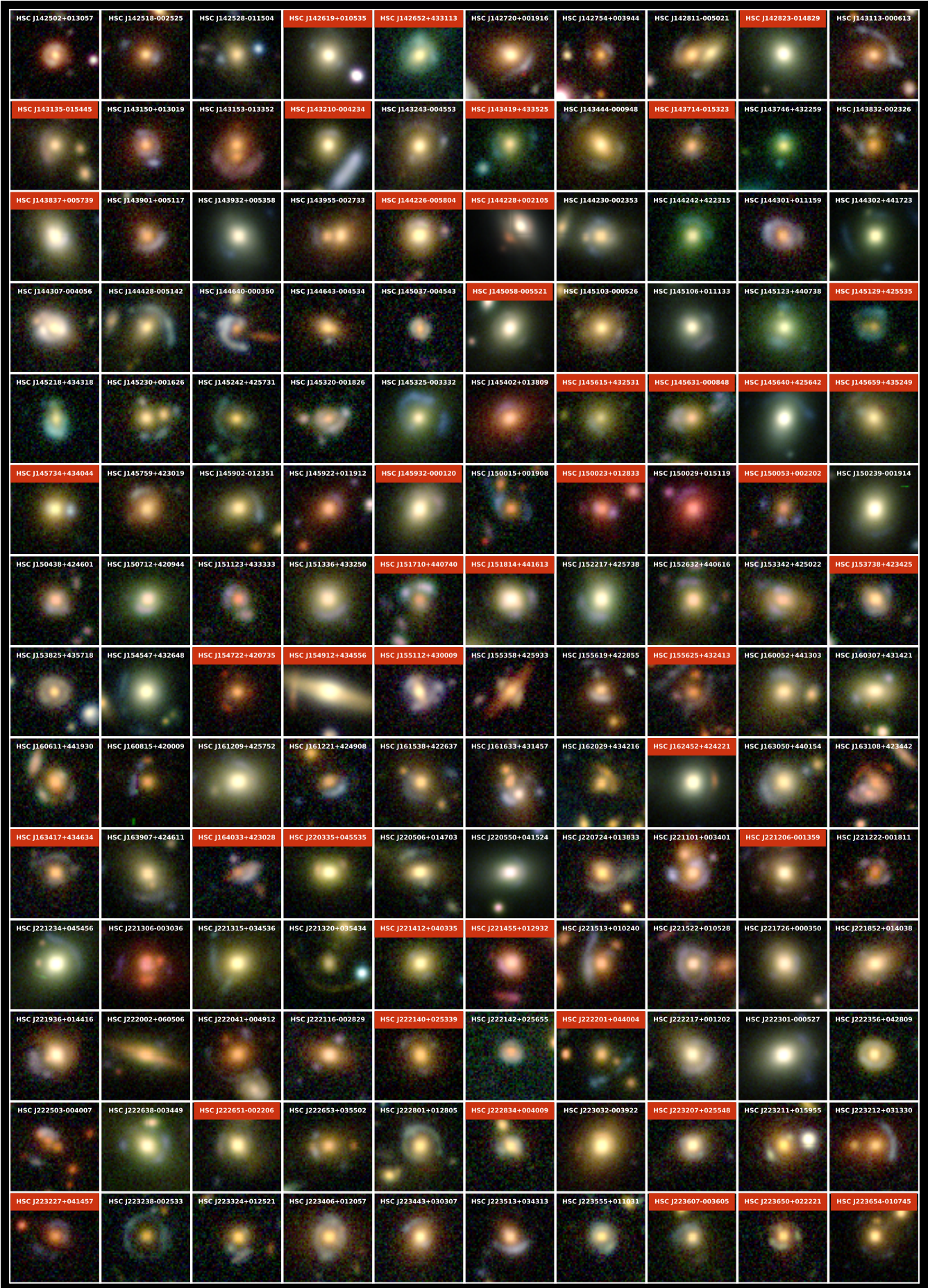


Fig. B.1: continued



Fig. B.1: continued